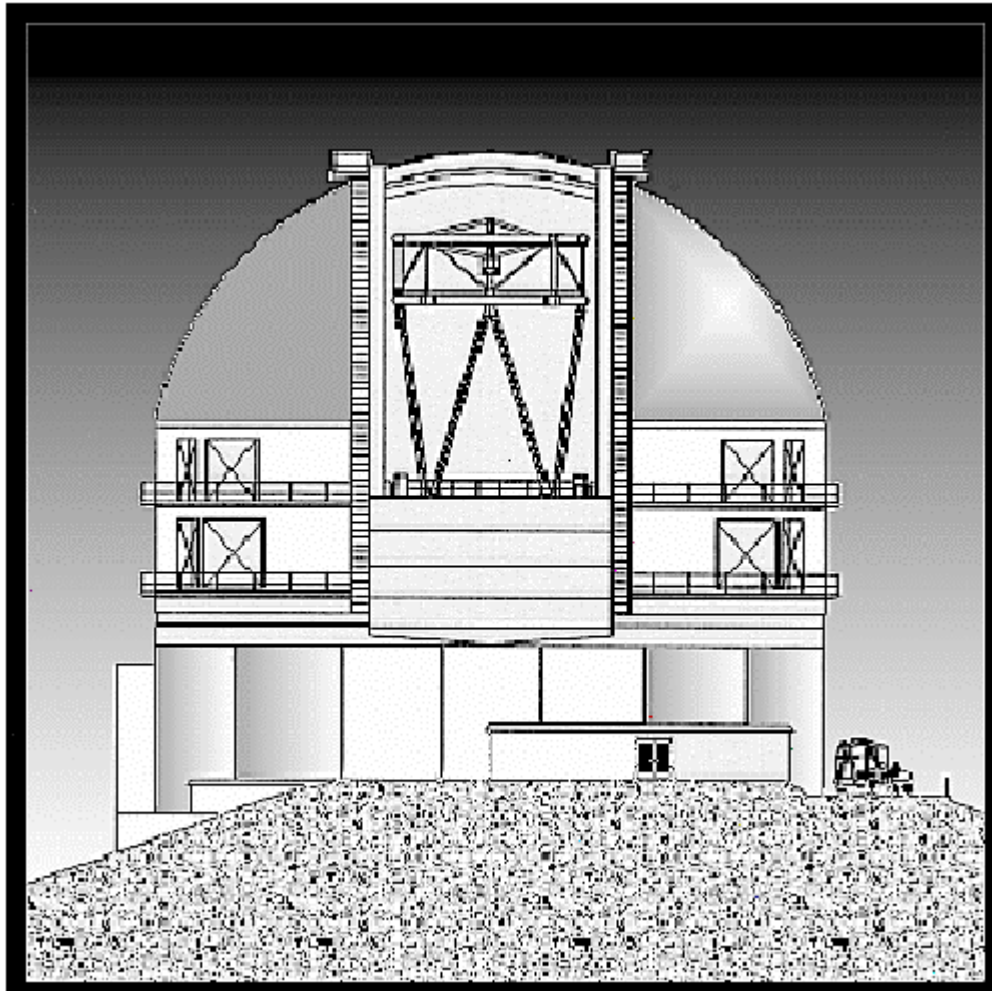




**GEMINI**  
8-M Telescopes  
Project

**RPT-O-G0047**

## **Gemini Telescopes f/16 Optical Design Summary**



**E. Hansen**  
Optics Group

July 6, 1994

GEMINI PROJECT OFFICE      950 N. Cherry Ave.      Tucson, Arizona 85719  
Phone: (520) 318-8545      Fax: (520) 318-8590

## TABLE OF CONTENTS

<b>1. DEFINITIONS AND TERMS .....</b>	<b>4</b>
<b>2. TELESCOPE CONFIGURATION.....</b>	<b>6</b>
2.1. COORDINATE SYSTEM. ....	6
2.2. IR OPTIMIZED TELESCOPE DESIGN. ....	6
2.3. IR TELESCOPE PRESCRIPTION. ....	7
2.4.1. <i>Motions of the Focal Plane</i> .....	7
2.4.2. <i>Motions of the Primary</i> .....	8
2.4.3. <i>Motions of the Secondary</i> . ....	8
2.5. PUPIL LOCATIONS.....	9
2.6. SEEING LAYER LOCATIONS. ....	9
2.7. M1 OPTICAL SURFACE DESCRIPTION.....	9
2.7.1. <i>M1 Polishing Specification</i> .....	9
2.7.2. <i>Departure of M1 Surface From a Best Fit Sphere and Parabola</i> . ....	9
2.8. M2 IR OPTICAL SURFACE DESCRIPTION.....	10
2.8.1. <i>M2 IR Polishing Specification</i> . ....	11
2.8.2. <i>Departure of M2 Surface from a Best Fit Sphere</i> .....	11
2.9. VISIBLE TELESCOPE DESIGN. ....	11
2.10. M2 VISIBLE OPTICAL SURFACE DESCRIPTION.....	11
3.2. SYSTEM PERFORMANCE, PRIME FOCUS. ....	13
3.3. ATMOSPHERIC DISPERSION, EFFECTS OF. ....	25
3.4. MISALIGNMENT INDUCED ABERRATIONS, M2. ....	27
3.4.1. <i>Axial Misalignment</i> .....	27
3.4.2. <i>Lateral Misalignment</i> .....	28
3.5. CHOPPING MOTION INDUCED ABERRATIONS. ....	30
3.6. IMAGE SMEAR DUE TO M2 MOTION. ....	30
3.7. ACTIVE CORRECTION USING M2. ....	31
3.8. OFF AXIS GUIDING. ....	32
3.9. PLATE SCALE. ....	32
3.10. DISTORTION AND ASTIGMATISM. ....	32
3.11. FIGURE ERRORS, EFFECTS ON IMAGE QUALITY. ....	33
3.12. REPEATING SURFACE DEFORMATIONS (PRINT-THROUGH), EFFECTS ON IMAGE QUALITY. ....	34
<b>4. STRAY LIGHT .....</b>	<b>35</b>
4.1. EMISSIVITY. ....	35
4.2. BAFFLES.....	35
4.3. VIGNETTING.....	36
<b>5. ACKNOWLEDGMENTS. ....</b>	<b>37</b>
<b>6. REFERENCES.....</b>	<b>37</b>
<b>APPENDIX A.....</b>	<b>38</b>
<b>APPENDIX B.....</b>	<b>41</b>
<b>APPENDIX C.....</b>	<b>46</b>

## **Preface**

This document describes the optical design of the Gemini 8-m telescopes in the f/16 configuration. A great deal of work has been done to characterize the optical properties of the telescopes. Sources include work done by the Gemini staff, those in partner countries as well as subcontracted studies. This report attempts to summarize the conclusions of the work done to date and provide a useful reference document.

The body report is divided into three sections, telescope configuration, Image quality, and stray light. The configuration section includes information on the optical properties of the telescopes as well as a detailed description of their optical components. The image quality section contains information on the imaging properties of the telescopes under various conditions. The last section describes the emissivity and stray light rejection of the telescopes based on the current design concepts for optics and baffling.

The information is organized and indexed by topic within each section of the report. This format was adopted to allow easy location of specific material as well as simplifying the addition of material as further studies are completed. A glossary and listing of references is also included.

## 1. DEFINITIONS AND TERMS

**Active Optics.** The term "Active optics" refers to the active force adjustment of the primary mirror supports to control the mirror's shape.

**Cassegrain rotator.** The "Cassegrain rotator" is defined as the equipment that provides a mounting for instruments. The cassegrain rotator rotates the instruments relative to the primary mirror as the telescope tracks to cancel the field rotation inherent in altitude azimuth-telescope mounts.

**Chopping.** "Chopping" is the procedure of tip-tilting the secondary mirror in a repetitive pattern to provide an image location shift for infrared background cancellation.

**Conic Constant ("K").**  $K = -e^2$ , where e equals the eccentricity of any conic section.

**Emissivity, Telescope.** The "Telescope emissivity" is defined as the ratio of unwanted energy in the focal plane as compared to the energy that would be directed at the focal plane from a unit emissivity secondary mirror.

**Field Angle.** The "Field Angle" is defined as the angle between an object and the optical axis of the telescope.

**Field Diameter.** The "Field Diameter" is defined as the angular extent of the full field .

**Figuring.** "Figuring" is the process whereby the shape of an optical surface is altered.

**Generating; Generation.** "Generating," or "Generation," is the process used for the rapid removal of glass by fixed abrasive grinding.

**IR System.** The "IR System" refers to the f/16 telescope using the IR secondary mirror.

**M1.** "M1" refers to the primary mirror

**M2.** "M2" refers to the secondary mirror

**Neutral point (zero coma point).** The "Neutral point" is defined as a point around which the secondary mirror can be rotated without introducing third order coma into the telescope wavefront.

**Null Corrector.** A "Null Corrector" is an optical system used in the optical testing of an aspheric surface. It converts a spherical wavefront into one that precisely matches the surface under test.

**Paraxial Radius of Curvature.** The "Paraxial Radius of Curvature" is the radius of curvature of a region of the projected Mirror surface immediately surrounding the optical axis.

**Polishing.** "Polishing" is the optical fabrication process that puts a highly finished, smooth and apparently amorphous surface on the Mirror.

**Prime focus.** The "Prime focus" is defined as the focal location for the primary mirror when it is used alone without a secondary mirror.

**Principal Focus.** The "Principal focus" is defined as the focal location when using both primary and secondary mirrors.

**Tip-tilt.** Tip-tilt is defined as rotation of the secondary mirror to correct for telescope misalignments or wavefront errors.

**Visible System.** The "Visible System" refers to the f/16 telescope using the visible secondary mirror, where the primary mirror forms the system stop.

**Vignetting.** "Vignetting" is defined as the reduction in total focal plane illumination due to a limiting aperture other than the system stop.

**Zenith angle.** The "Zenith angle" is defined as the angle between vertical and the optical axis of the telescope.

## 2. TELESCOPE CONFIGURATION

### 2.1. COORDINATE SYSTEM.

The local coordinate axes used in this document form a right handed system. The X axis is parallel to the telescope elevation axis, positive from left to right looking at the primary mirror optical surface with the telescope horizon pointing. The Z axis is parallel with the optical axis, positive from the primary mirror to the secondary mirror. The origin of this coordinate system is defined to be at the vertex of the optical surface of the primary mirror.

### 2.2. IR OPTIMIZED TELESCOPE DESIGN.

The fundamental parameters describing the telescope are listed below;

system focal length    128 meters  
 entrance pupil diameter    7.9 meters  
 primary mirror focal ratio    1.8  
 back focal distance    4.0 meters behind the primary mirror vertex  
 unvignetted field diameter..... 3.5 arc minutes (without chopping).

The f/16 IR optimized optical system is shown in figure 1. In the f/16 configuration the system is being operated as a modified Richey-Chretien telescope, which is the aplanatic version of the cassegrain telescope. While the primary mirror is being figured with a conic constant optimized for f/16 operation, the system will also be capable of operation with other secondary mirror focal ratios or at a prime focus. Refiguring of the primary to a paraboloid using active optics will allow operation at prime focus or as a Classical Cassegrain telescope<sup>1</sup>. With a different secondary mirror, the conic constant of the primary mirror can also be adjusted to produce a Richey-Chretien telescope at something other than f/16.

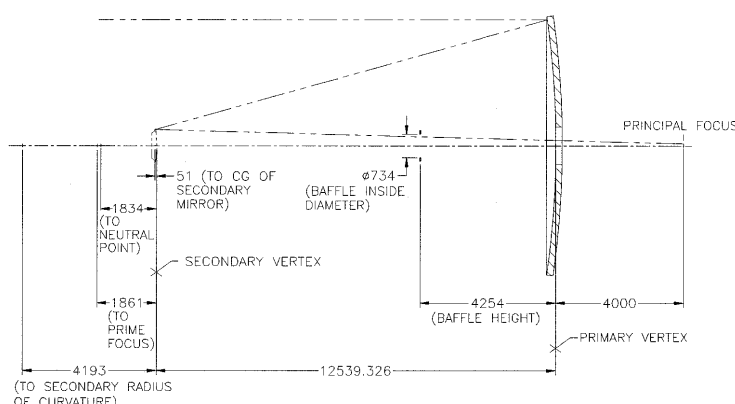


Figure 1  
 (dimensions in mm)

The choice of secondary mirror focal ratio was a compromise between two conflicting goals.

First, to reduce Petzval curvature and ease instrument design complexity, a small focal ratio was desirable. However, a small focal ratio would require a large secondary mirror when keeping the focal plane location constant. And as secondary mirrors increased in size, the problem of maintaining low self-weight deflection in changing gravity orientations became more difficult. The best overall compromise was found to be an f/16 system which yields a focal surface radius of curvature of 1.915 meters. The 1.022 meter diameter optical surface of the infrared optimized secondary mirror contains a 0.169 meter diameter central hole minimizing the non-sky reflecting surfaces seen by infrared instruments. The inner and outer diameters form the system stop, resulting in a primary mirror diameter of 7.9846 meters with a 3.5 arcminute diameter field.

### 2.3. IR TELESCOPE PRESCRIPTION.

Appendix A contains a CodeV listing of the f/16 IR optical prescription.

### 2.4. LINE OF SIGHT RELATIONSHIPS.

The Gemini pointing philosophy may be summed up as, *The Cassegrain rotator axis defines the pointing axis of the telescope.* The implications of this philosophy are detailed below. The effect of motions of the focal plane, primary mirror, and secondary mirror relative to the Cassegrain rotator axis and motions of the Cassegrain rotator axis relative to its frame of reference have been examined<sup>2</sup>, and are reported here.

#### 2.4.1. MOTIONS OF THE FOCAL PLANE.

The motions of the focal plane relative to the Cassegrain rotator axis (CR) which will cause pointing errors are, translation in X or Y relative to CR and rotation about the Z axis relative to the CR. Small amounts of tip/tilt of the focal plane relative to the CR and piston relative to the CR do not cause pointing errors.

Translation of the focal plane relative to the CR will cause the following pointing error;

$$R = -0.0016T_f$$

with, R = Pointing error in arcseconds  
T<sub>f</sub> = Focal plane translation in microns

so a translation of the focal plane by 100 microns will cause a pointing error of -0.16 arcseconds. The negative sign on the pointing error means that, if the focal plane translates in the -Y direction as the telescope points away from the zenith, the image moves in the +Y direction in the focal plane.

Rotation of the focal plane relative to the CR will cause the following shift in off axis images;

$$R = .00029Z_fF$$

with, Z<sub>f</sub> = Focal plane rotation in arcseconds  
F = Image field angle in arcminutes

A rotation of the focal plane by 100 arcseconds at a 10 arcminute radius produces an image shift of .29 arcseconds radially opposite the direction of rotation of the focal plane.

#### 2.4.2. MOTIONS OF THE PRIMARY.

The motions of the primary relative to the CR which will cause pointing errors are translation in X/Y relative to CR and tip/tilt around X/Y relative to CR. Rotation about the Z axis relative to the CR and piston relative to the CR do not cause pointing errors.

Translation of the primary relative to the CR will cause the following pointing error;

$$R = 0.0143T_p$$

with,  $T_p$  = Translation of M1 in microns

A translation of the primary by 100 microns will cause a pointing error of 1.43 arcseconds. The lack of a negative sign on the relation means that the motion of the image in the focal plane and the direction of motion of the primary are in the same direction.

Tilt of the primary relative to the CR will cause the following pointing error;

$$R = \pm 2.0R_p$$

with,  $R_p$  = Tilt of M1 in arcseconds

A tilt of the primary of 1 arcsecond will cause a pointing error of 2 arcseconds.

#### 2.4.3. MOTIONS OF THE SECONDARY.

The motions of the secondary relative to the CR which will cause pointing errors are translation in X/Y relative to CR and tip/tilt around X/Y relative to CR. Rotation about the Z axis relative to the CR and piston relative to the CR do not cause pointing errors.

Translation of the secondary relative to the CR will cause the following pointing error;

$$R = -0.0127T_s$$

with,  $T_s$  = Translation of M2 in microns

A translation of the secondary by 100 microns will cause a pointing error of -1.27 arcseconds. The negative sign on the relation means that the motion of the image in the focal plane and the direction of motion of the secondary are in opposite directions.

Tilt of the secondary about its vertex relative to the CR will cause the following pointing error;

$$R = \pm 0.2584R_s$$

with,  $R_s$  = Rotation of M2 in arcseconds

A tilt of the secondary of 1 arcsecond will cause a pointing error of 0.2584 arcseconds.

## 2.5. PUPIL LOCATIONS.

In the IR optimized telescope the secondary mirror forms the system stop and defines the exit pupil. The entrance pupil is 7.9 meters in diameter and located 112.625 meters behind the principal focus.

The visible telescope stop is formed by the primary mirror aperture with an exit pupil of 1.15 meter diameter located 1.8 meters behind the secondary mirror.

## 2.6. SEEING LAYER LOCATIONS.

Seeing layer locations of between 0 and 10 Km above the Mauna Kea site have been used for Gemini adaptive optics studies, with 4 Km height being the most common assumption. The conjugate positions in image space are;

Seeing Layer Height	Image Position
4 Km	523.2 cm behind the principal focus
10 Km	179.4 cm behind the principal focus

## 2.7. M1 OPTICAL SURFACE DESCRIPTION.

Parameters describing the optical surface are listed below;

radius of curvature..... 28.80 m  
 conic constant..... -1.003756  
 outside diameter ..... 8.10 m  
 inside diameter ..... 1.18 m  
 outside clear aperture..... 8.00 m  
 inside clear aperture..... 1.20 m

### 2.7.1. M1 POLISHING SPECIFICATION.

The M1 polishing specification is given in Appendix B

### 2.7.2. DEPARTURE OF M1 SURFACE FROM A BEST FIT SPHERE AND PARABOLA.

The primary surface shape is optimized for an f/16 telescope configuration, with a conic constant of -1.00376. The departure of this surface from a best fit sphere, radius 28.94191 meters is shown in Figure 2. The departure of the surface from a best parabola, radius 28.80053 meters is shown in Figure 3.

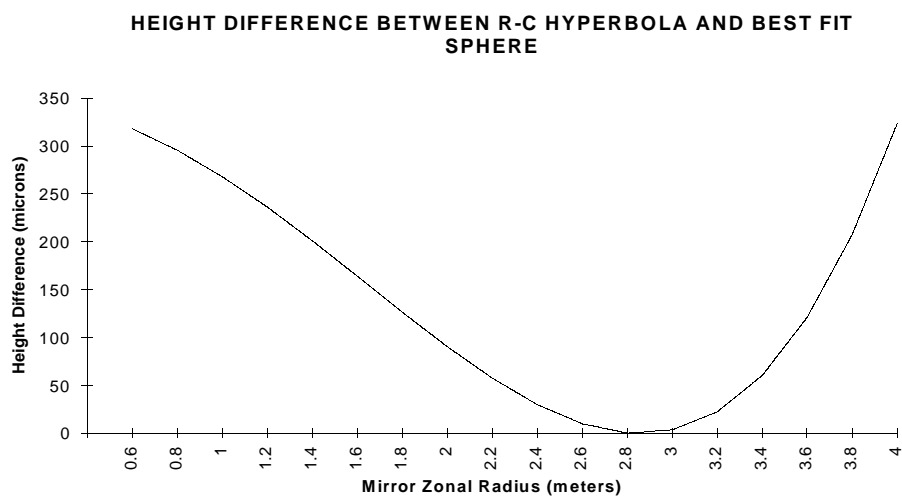


Figure 2

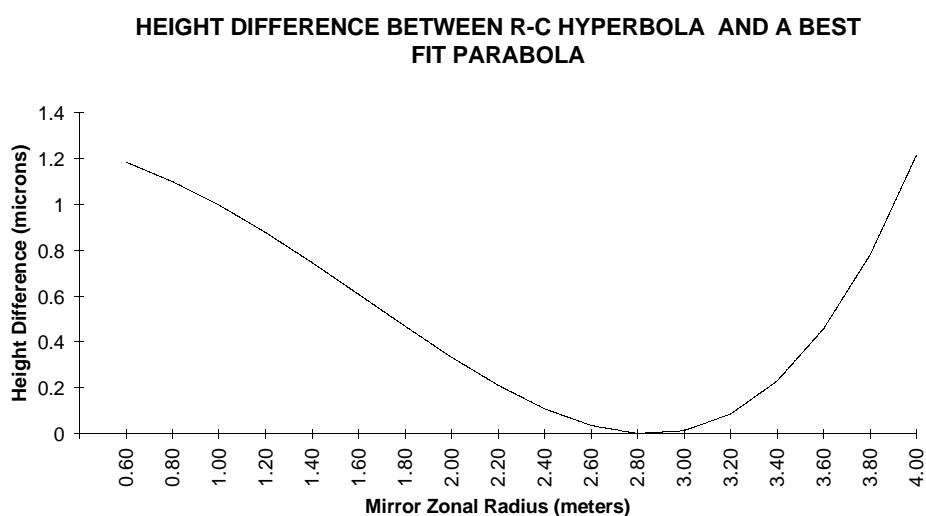


Figure 3

## 2.8. M2 IR OPTICAL SURFACE DESCRIPTION.

The following parameters describe the theoretical M2 optical surface:

radius of curvature ..... 4.1930685 m  
 conic constant ..... -1.612898  
 outside diameter ..... 1.023 m  
 inside diameter ..... 0.168 m  
 outside clear aperture ..... 1.022 m  
 inside clear aperture ..... 0.169 m

### 2.8.1. M2 IR POLISHING SPECIFICATION.

The proposed M2 polishing specification is given in Appendix C.

### 2.8.2. DEPARTURE OF M2 SURFACE FROM A BEST FIT SPHERE.

The secondary surface shape is optimized for an f/16 telescope configuration, with a conic constant of -1.612898. The departure of this surface from a best fit sphere, radius 4.2185 meters is shown in figure 4.

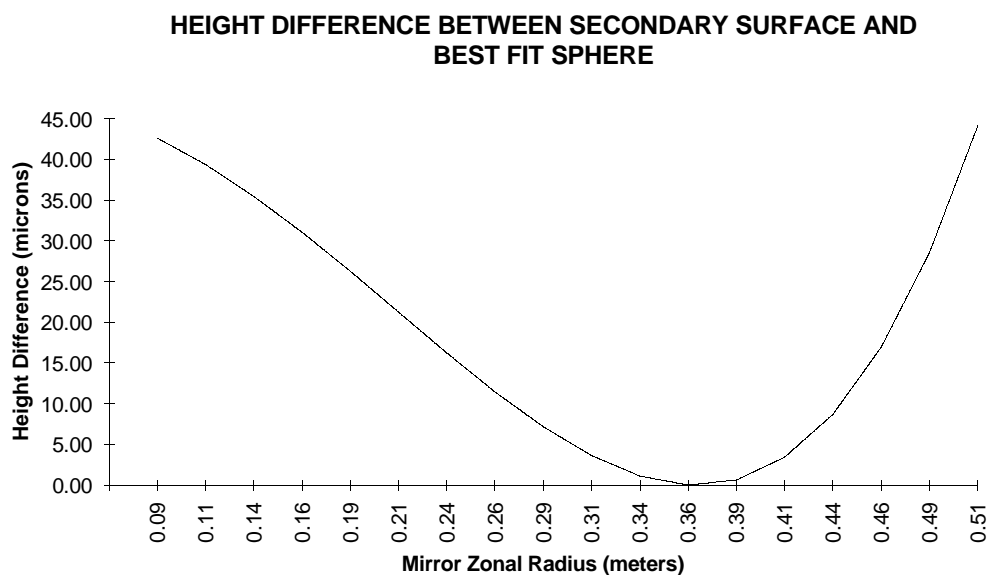


Figure 4

### 2.9. VISIBLE TELESCOPE DESIGN.

The telescope is transformed to the f/16 visible configuration by a change of secondary mirrors. This configuration allows a higher transmittance in the visible wavelengths with the use of an aluminum coating on the secondary mirror. The visible secondary is also oversized, moving the system stop to the 8.0 meter aperture of the primary.

### 2.10. M2 VISIBLE OPTICAL SURFACE DESCRIPTION.

The following parameters describe the theoretical M2 optical surface;

radius of curvature	-4.1930685 m
conic constant	-1.612898
outside diameter	1.102 m
clear aperture	1.082 m diameter

### 2.11. VISIBLE USE OF IR TELESCOPE DESIGN.

The telescope IR configuration may be used for visible observations by deploying a secondary baffle which blocks direct illumination of a 12 arcminute field diameter. The vignetting of this configuration is described in section 4.3. is transformed to the f/16 visible configuration by a change of secondary mirrors. The reflectance of silver coatings at visible wavelengths is shown in Figure 5.

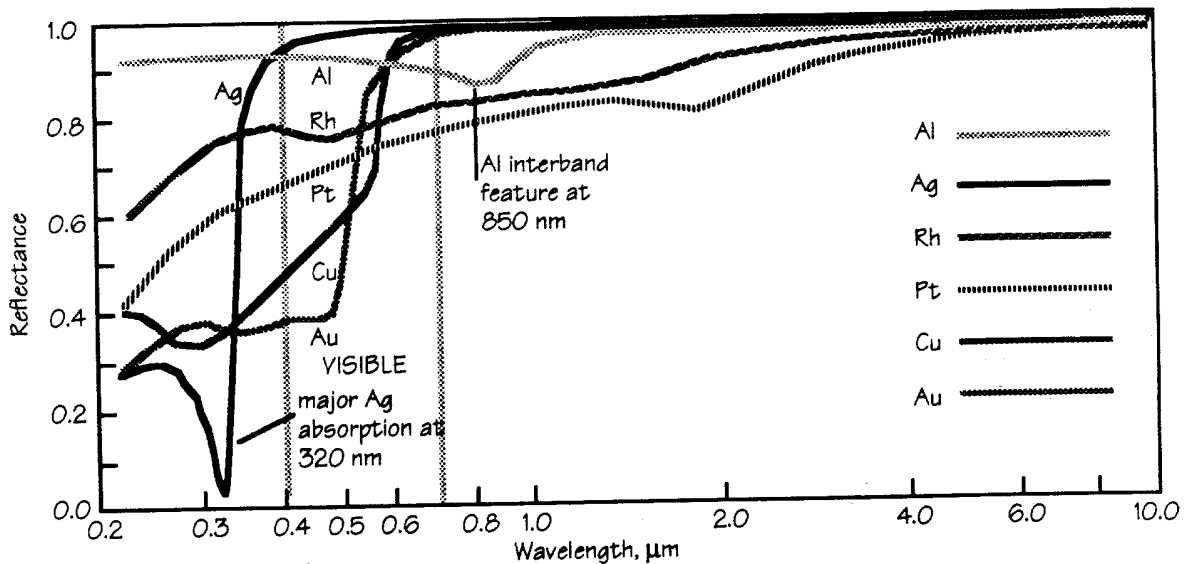


Figure 5 Reflectance of Ag

### 3. IMAGE QUALITY

#### 3.1. SYSTEM PERFORMANCE, CURVED AND FLAT FIELD.

The primary measure being used to judge telescope performance is encircled energy diameter. The percent encircled energy diameters used in the Gemini Error Budget<sup>3</sup> for 550, 2200, and 10000 nm wavelengths are given in Table 1. Figures 6, 7, and 8 show the encircled energy values for different field angles.

Wavelength in nanometers	36 % Encircled Energy	50 % Encircled Energy	85 % Encircled Energy	90 % Encircled Energy
550 nm	0.115	0.176	not used	.240
2200 nm	not used	0.065	.196	not used
10000 nm	not used	.300	not used	not used

Spot diagrams for both curved and flat fields are illustrated in Figures 9 and 10. These are shown through focus ( $\pm .5$ mm) and at various field angles. Note the difference in scale between Figures 9 and 10.

Optical path difference fans are given in Figure 11. The fans are given for two orthogonal directions at various field angles. The 3 arcminute field angle fan indicates a 0.35 micron P-V astigmatism. Previous studies have shown 1.36 microns P-V astigmatism present at a 6 arcminute field angle.

#### 3.2. SYSTEM PERFORMANCE, PRIME FOCUS.

The performance of the telescope was examined at prime focus assuming the active optics modified the mirror figure to a best fit paraboloid. Figures 12, 13 and 14 show the encircled energy values for 550, 2200, and 10000 nm wavelengths, on axis and at a field angle of 1.8 arcminutes.

Spot diagrams for the curved field configuration are illustrated in Figure 15. These are shown through focus ( $\pm .1$ mm) and at field angles of 0 and 1.8 arcminutes.

Optical path difference fans are given in Figure 16. The fans are given for two orthogonal directions at various field positions. The 1.8-arcminute field angle fan indicates substantial off-axis coma.

FIGURE 6

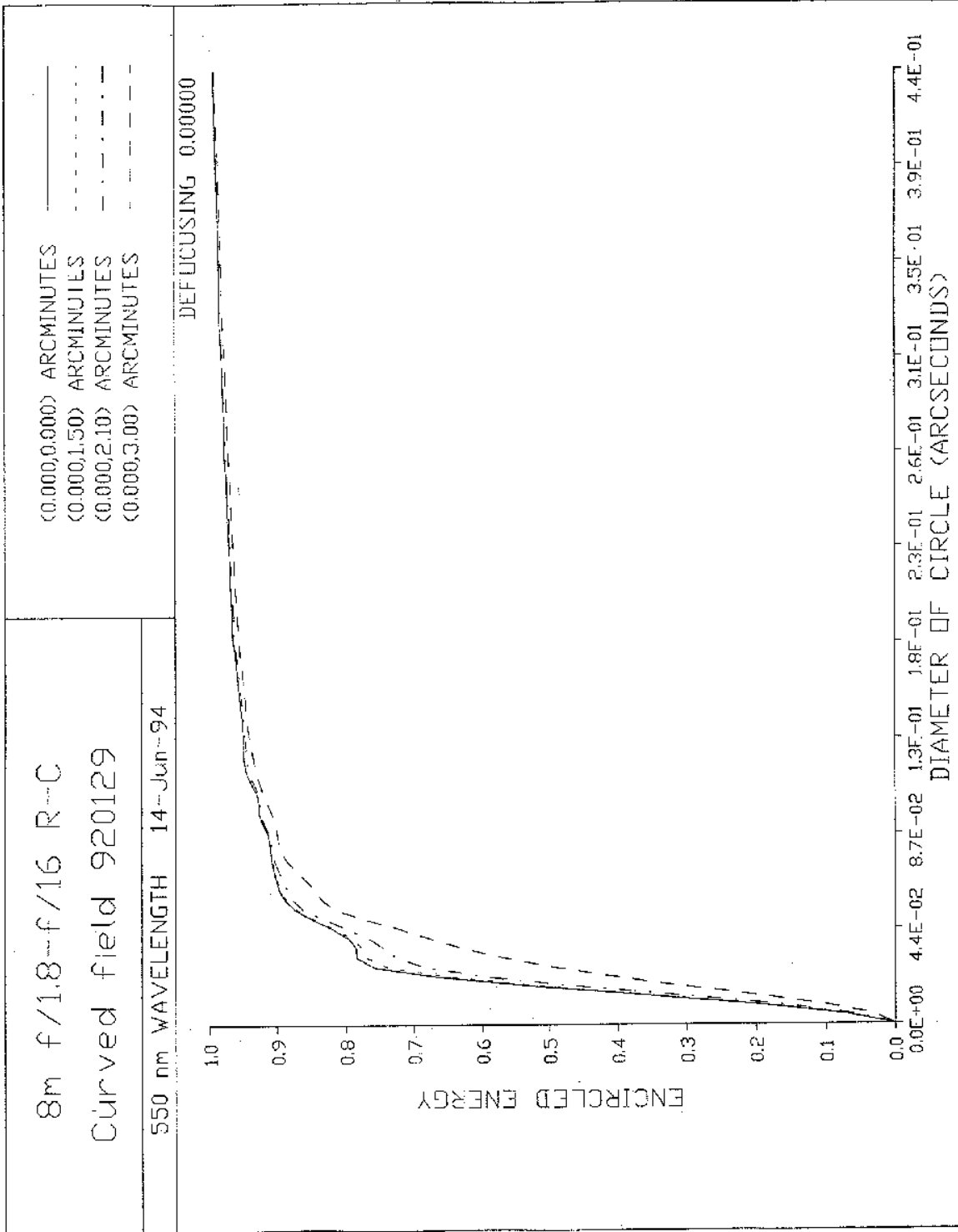


FIGURE 7

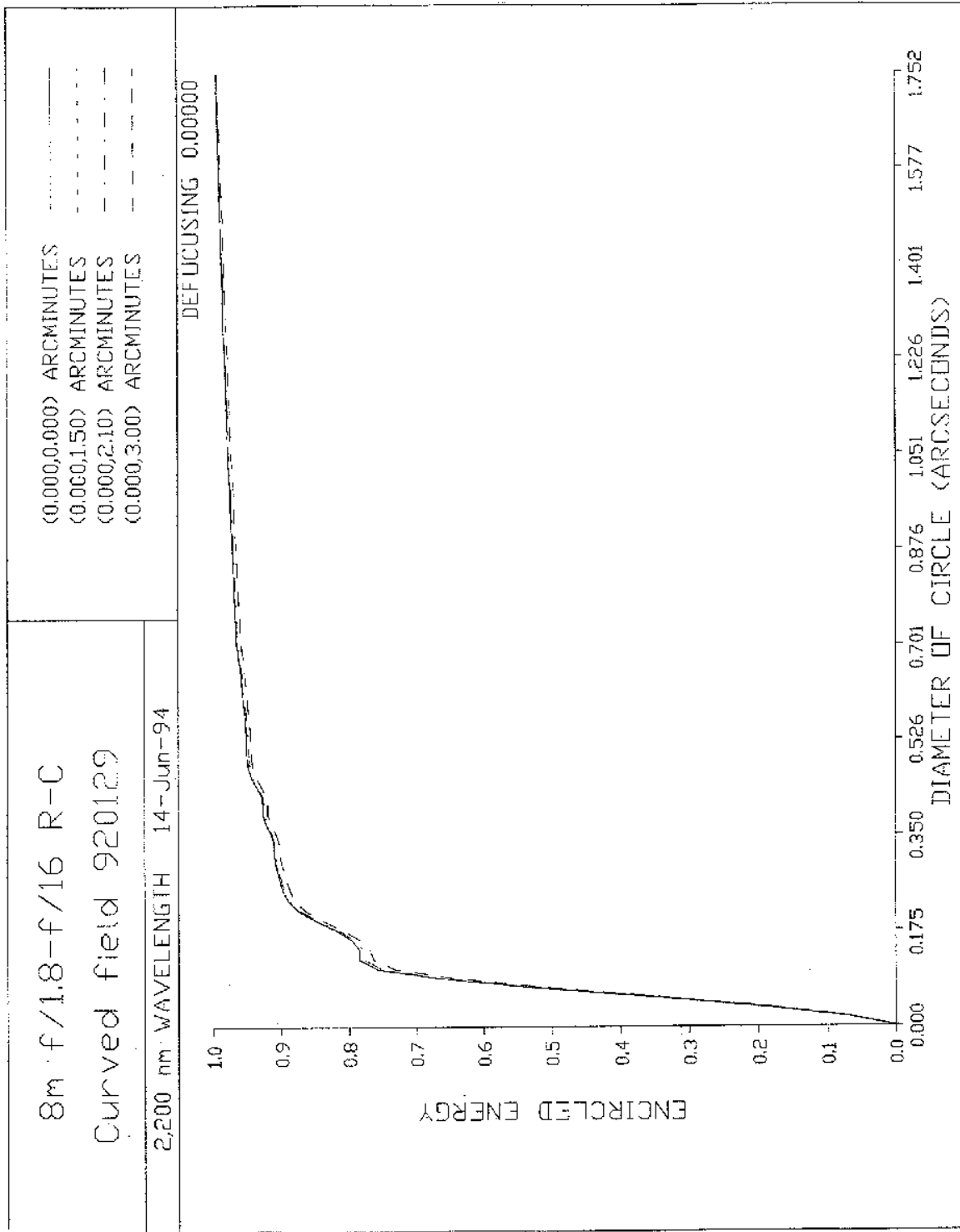


FIGURE 8

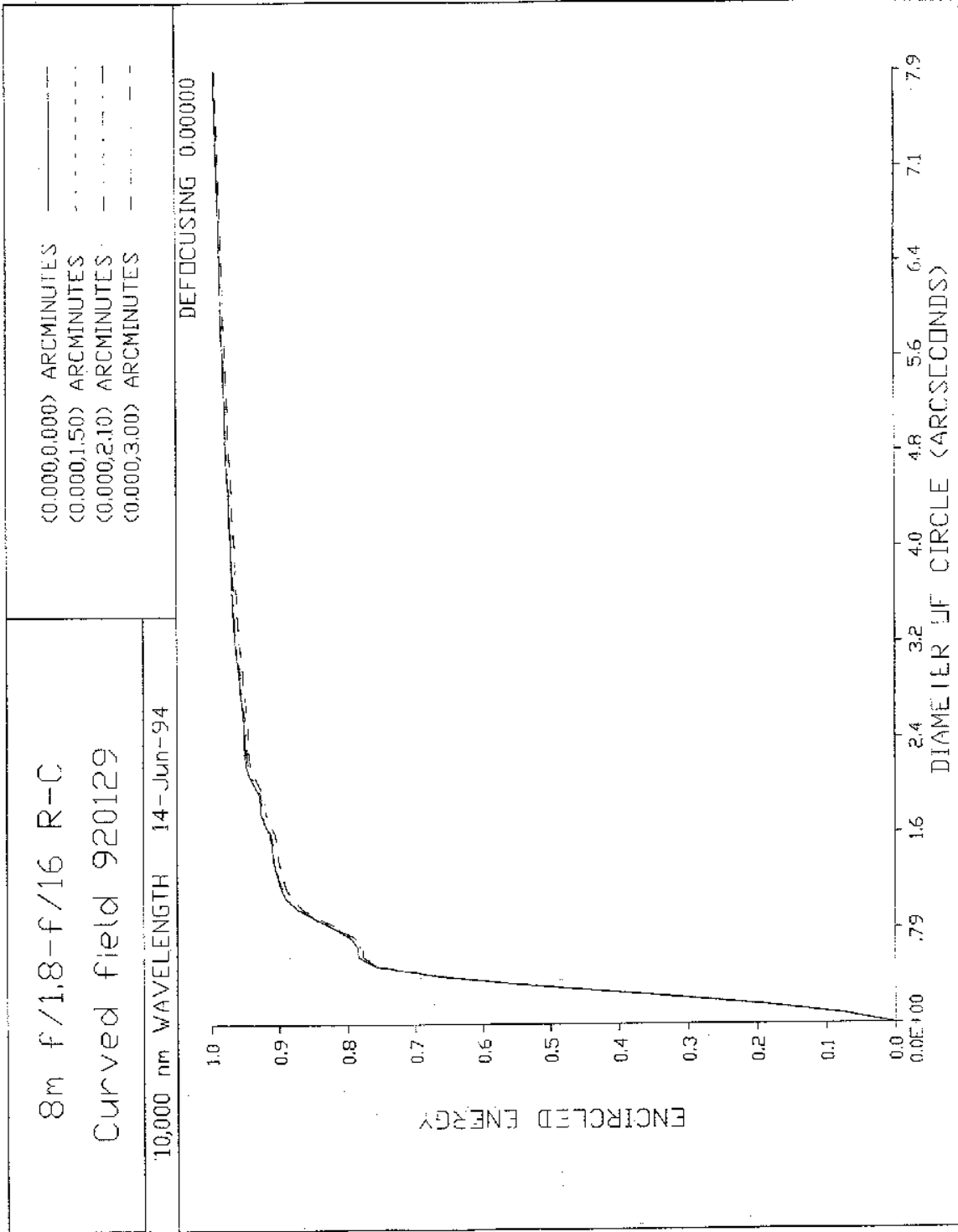


FIGURE 9

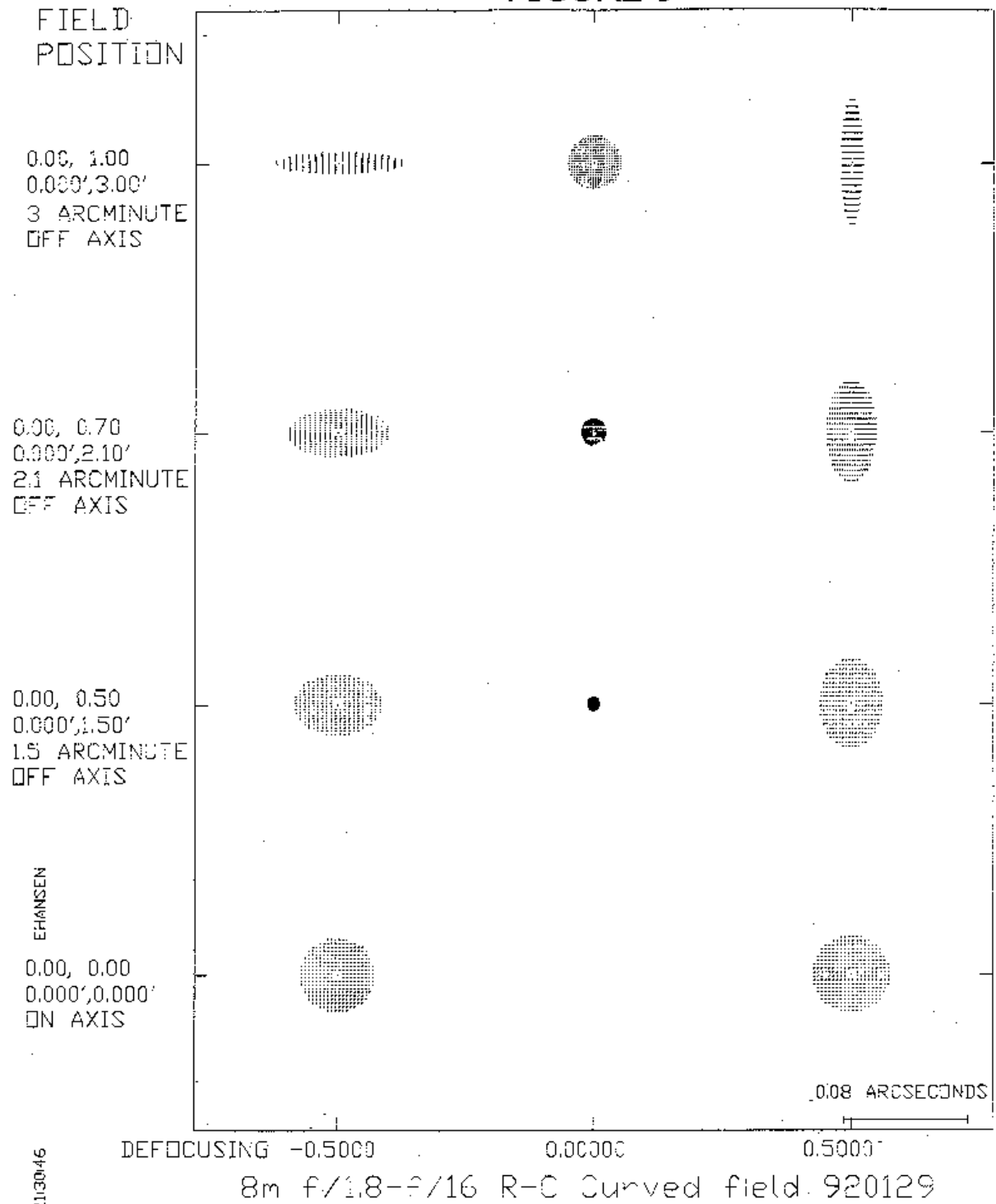
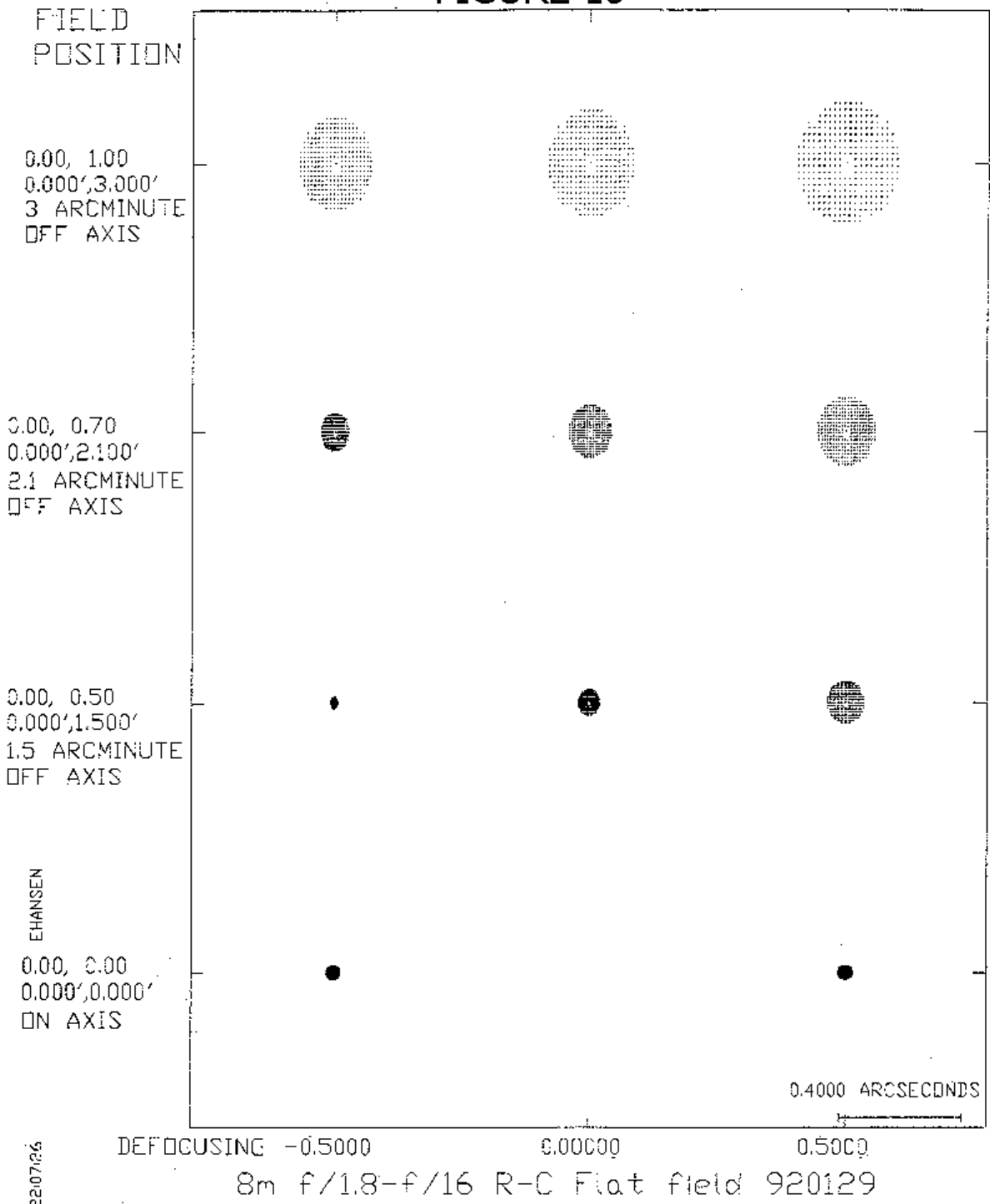


FIGURE 10



2207126

FIGURE 11

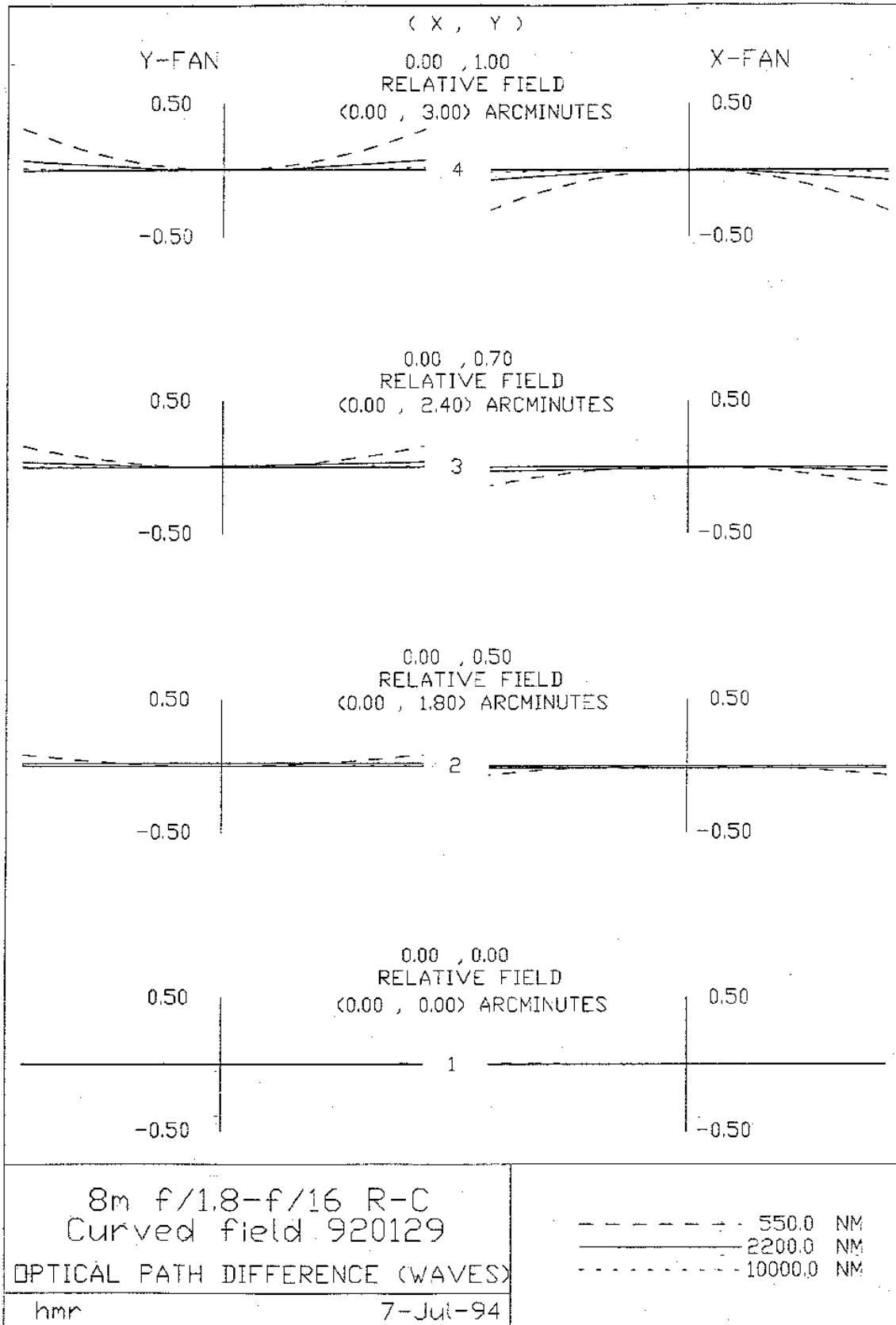


FIGURE 12

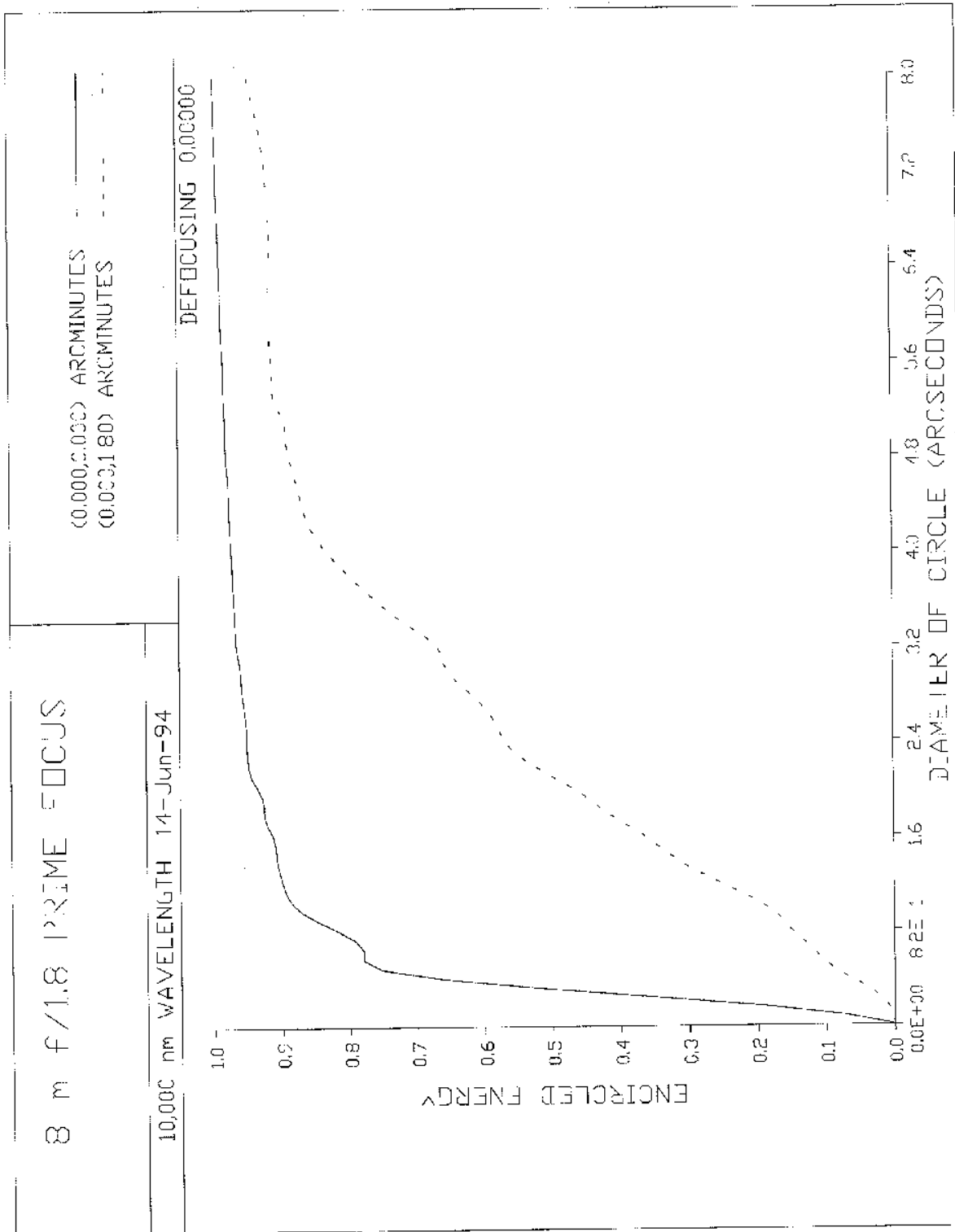


FIGURE 13

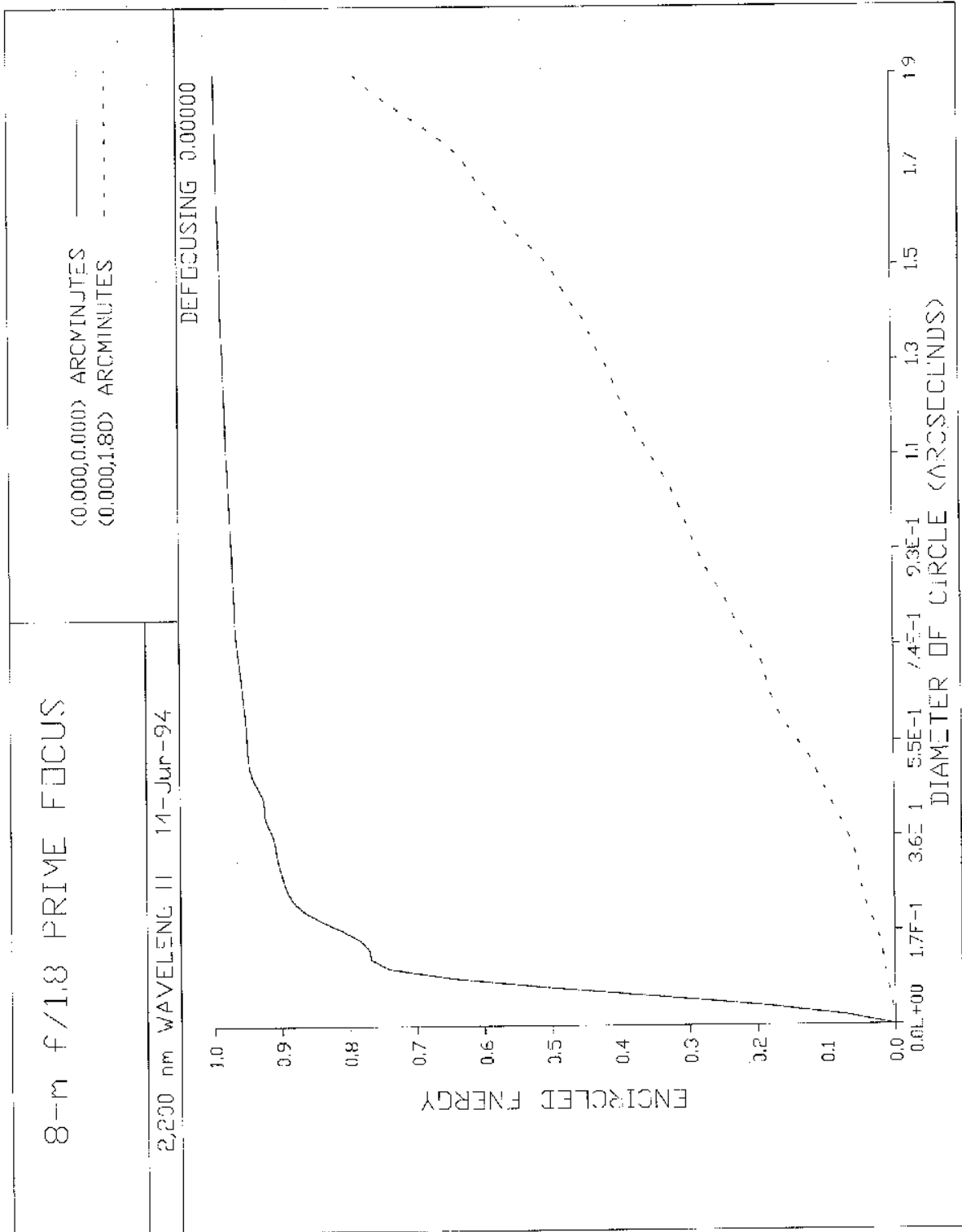


FIGURE 14

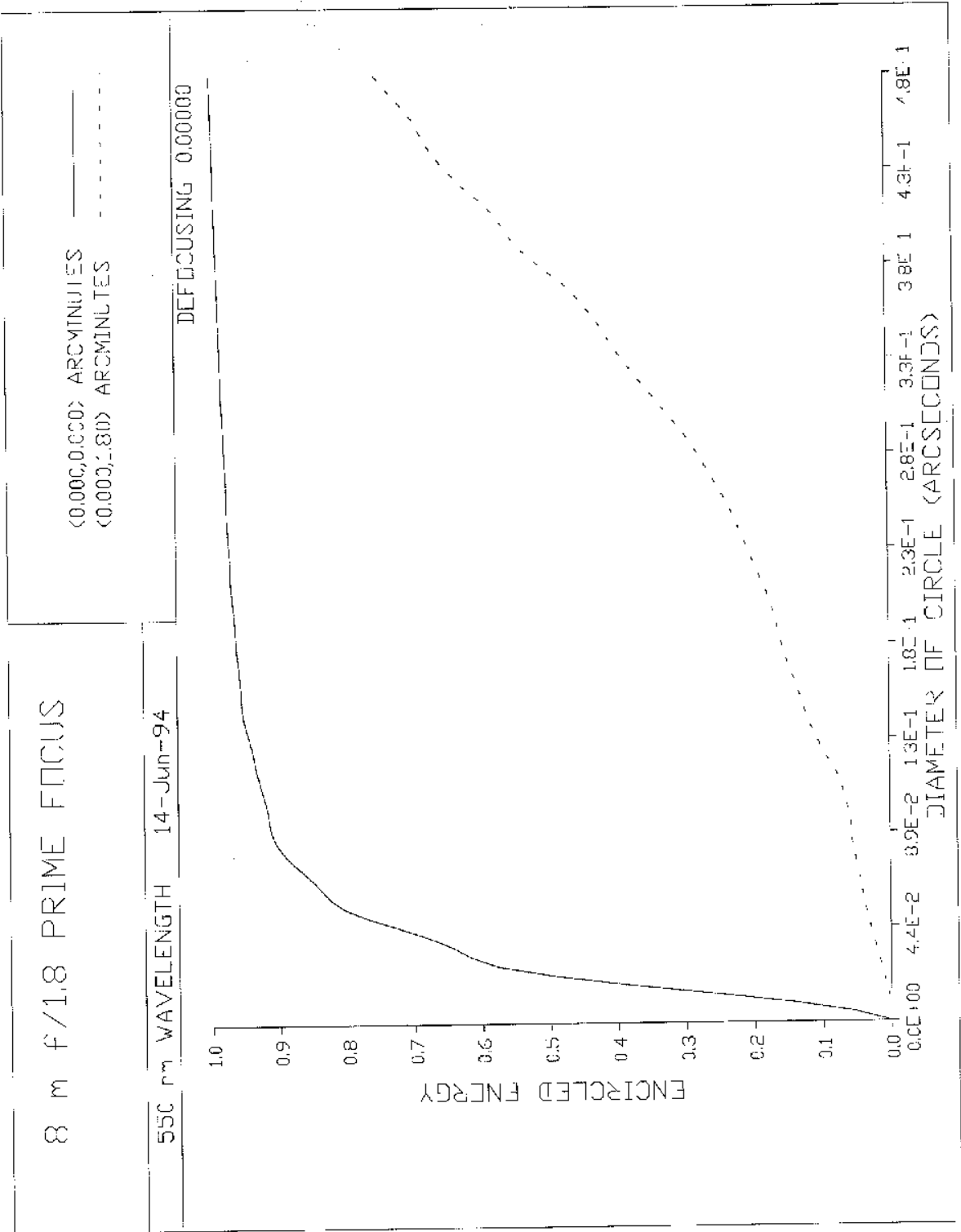


FIGURE 15

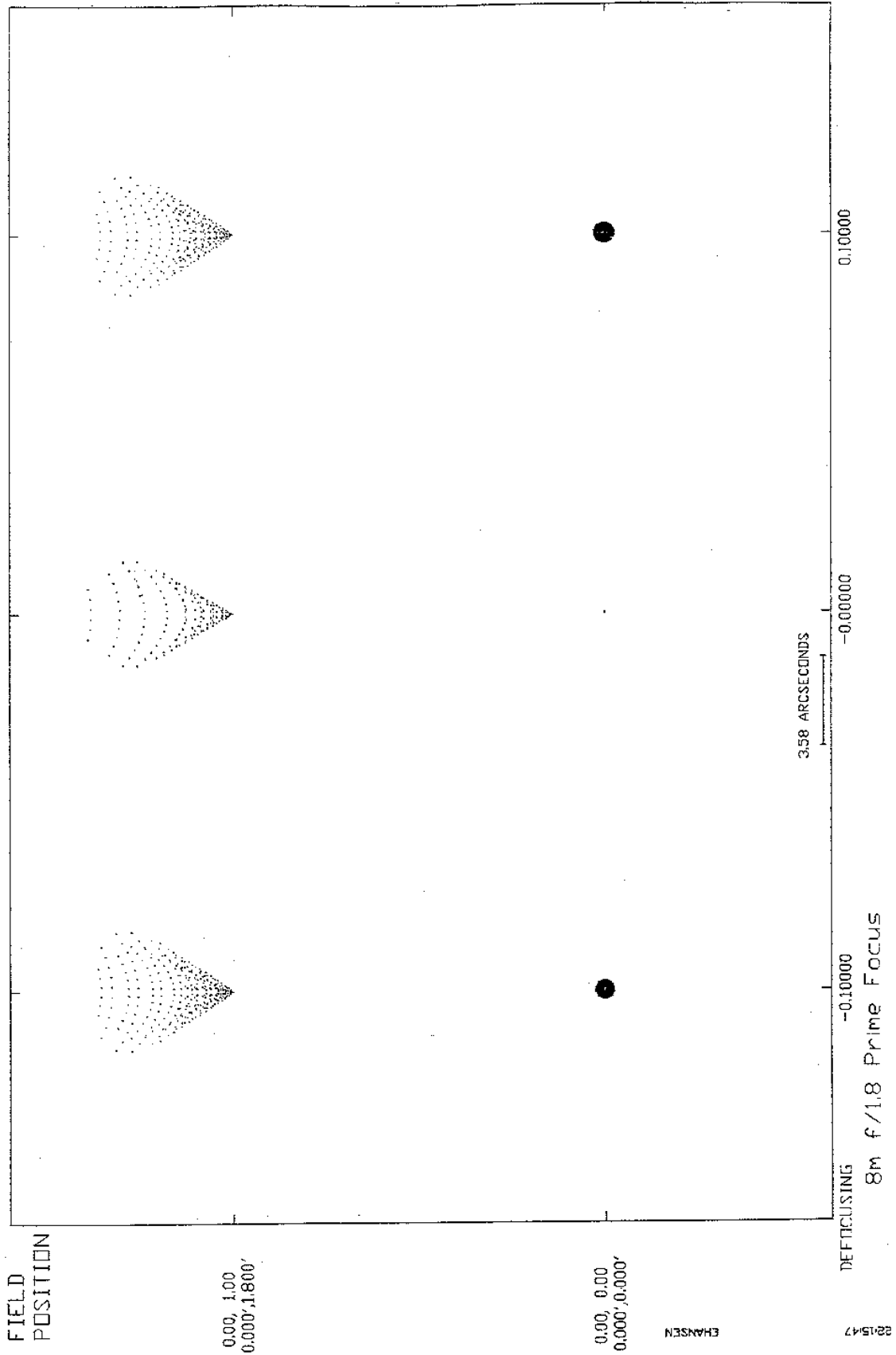
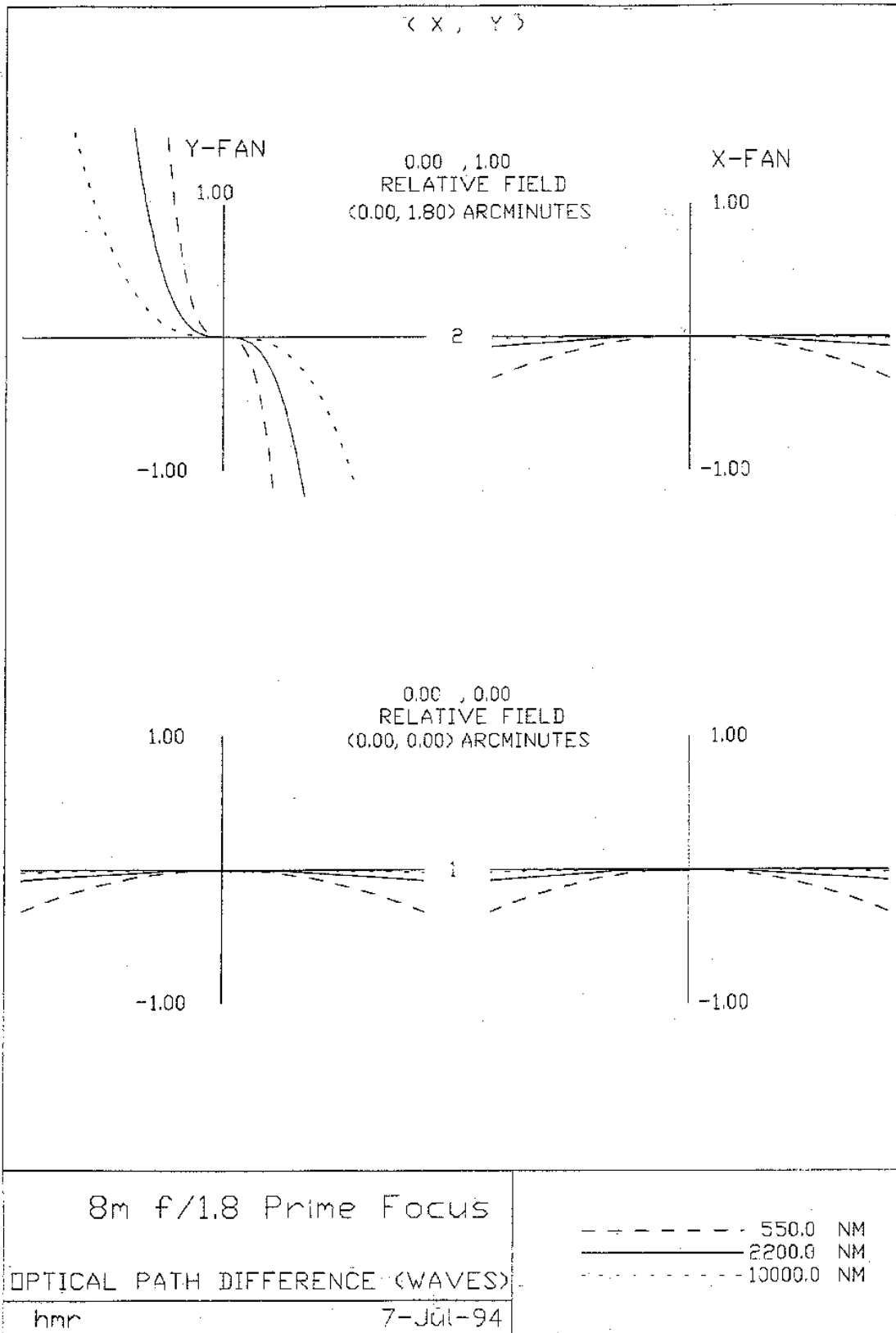


FIGURE 16

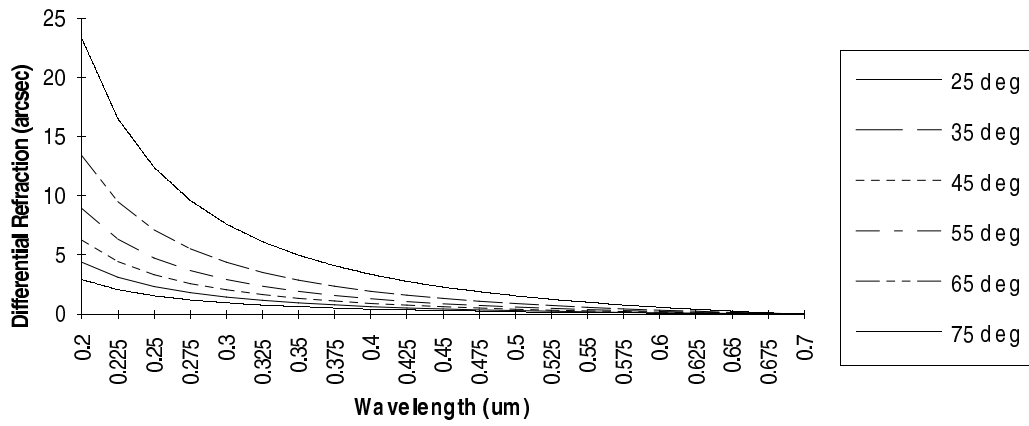


### 3.3 ATMOSPHERIC DISPERSION, EFFECTS OF.

The dispersion effects of the atmosphere, while small, act to spread the image of a point source. The spreading effect is proportional to the chromatic content of the source. The refractive index of air at the two sites can be modeled as a function of wavelength with corrections for temperature, pressure and water vapor content<sup>4</sup>. The results for Mauna Kea are presented in Figure 17 and results for Cerro Pachon are presented in Figure 18, both relative to a 0.7 micron wavelength image. The average environmental conditions used for this analysis are given in Table 2. It is clear that the importance of atmospheric dispersion increases rapidly with increasing zenith angle and decreasing wavelength. It is also clear that pointing correction will be required when changing zenith angle during tracking.

Table 2 Average Environmental Conditions		
	<b>Mauna Kea</b>	<b>Cerro Pachon</b>
<i>Atmospheric Pressure (mm Hg)</i>	454.0	544.0
<i>Temperature (C)</i>	2.0	7.0
<i>Water Vapor Pressure (mm Hg)</i>	4.0	4.0

### Atmospheric Dispersion Mauna Kea



### Atmospheric Dispersion Mauna Kea

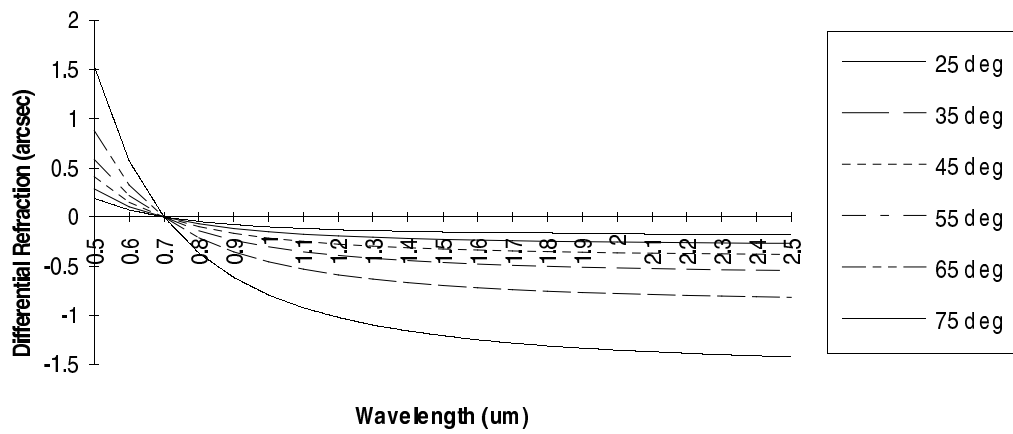


Figure 17

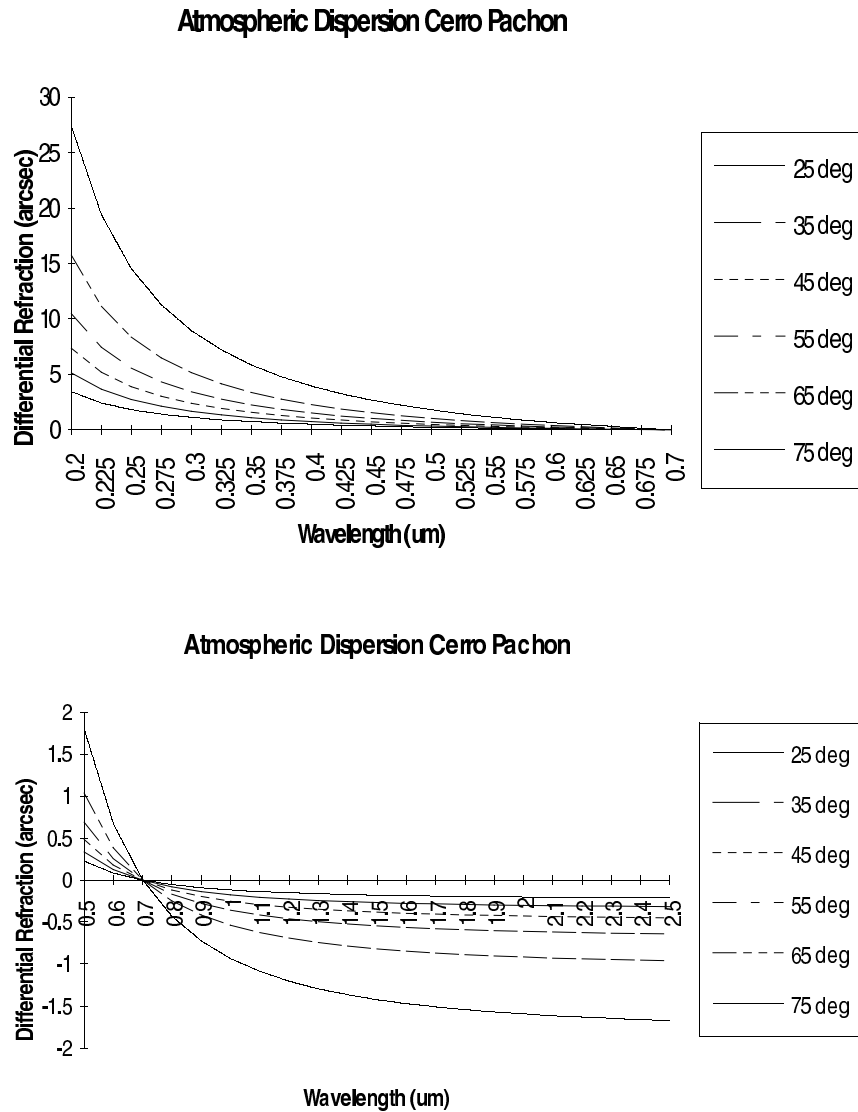


Figure 18

### 3.4 MISALIGNMENT INDUCED ABERRATIONS, M2.

Secondary misalignment is of interest because it can produce wavefront errors and changes in image scale. The effects of secondary misalignment are well documented in optics literature<sup>5,6</sup>; major considerations are repeated here.

#### 3.4.1 AXIAL MISALIGNMENT.

Axial misalignment or despace is defined as the displacement of the secondary axially a distance  $dS$ , the sign being positive if separation increases. If the detector remains at the initial principle focus, two changes occur in the image. First the wavefront quality is degraded and second the image scale is changed. Changing the mirror spacing introduces both defocus and spherical

aberration. In practice if the detector is not repositioned, the defocus term is dominant and the RMS wavefront error in waves is given by;

$$W_d = \frac{(1-e^2)dS}{16\sqrt{3}\lambda F_p^2}$$

with, obscuration ratio =  $e$   
primary  $f/\# = F_p$

Plate scale change may be calculated from the paraxial image height change as;

$$dIS = ((adS(m^2(2+B)/m(1+B))-aFD_p)/-aFD_p)$$

with, plate scale change =  $dIS$   
field angle =  $a$   
system  $f/\# = F$   
primary diameter =  $D_p$   
secondary magnification =  $m = F/F_p$   
primary vertex to focus separation/primary focal length =  $B$

The paraxial image shift  $dZ$ , may be found from;

$$dZ = -m^2 dS$$

If  $dS$  remains constant during an exposure interval, only wavefront error factors can cause image degradation. If  $dS$  varies during the exposure, a change in image scale will cause the image to smear. If the image point on axis is held stationary with respect to the sensor, the image smear will be most noticeable at the outer edge of the image format. Under such circumstances, using a small field, the wavefront error effects will mask those due to image scale change. The exception to this is when using offset tracking. If the offset tracking star is far off axis, the entire image can be smeared by a change in image scale during an exposure. For example, if the guide star is 6 arcminutes off axis, a 100 ppm plate scale change results in an image smear of 0.3 arcseconds on axis.

### 3.4.2 LATERAL MISALIGNMENT.

Lateral misalignment involves a displacement of the secondary mirror off the system axis without any significant change in mirror spacing. Lateral misalignment will take the form of a tilt or decenter of the secondary mirror axis with respect to the primary mirror axis. This will introduce third order axial coma, and cause a lateral shift in the image position. Both tilt and decenter introduce the same form of axial coma, and it is possible to cancel out the coma introduced by a given tilt by decentering the secondary mirror appropriately. This combination of tilt and decenter is equivalent to rotating the secondary mirror axis about a fixed point  $P_{wo}$  on the primary mirror axis. That position, the neutral point, is a function of secondary mirror magnification and conic constant and is located between the prime focus and the secondary vertex.

Similarly, the image displacement caused by misaligning the secondary will be zero if the misalignment takes the form of a rotation about the center of curvature of the secondary. Therefore, lateral misalignment may be characterized by the separation of the two optical axes at the neutral point  $P_{wo}$  and the center of curvature Pcc. Axial coma is then proportional to the separation  $dY_{wo}$  and image displacement is proportional to the separation  $dY_{cc}$ .

The axial coma as expressed as an RMS wavefront error in waves is;

$$W_c = C_d dY_{wo}$$

where  $C_d$  is the misalignment coefficient. Based on third order analysis;

$$C_d = .0037(1+(1+B)/m^2(m-B))/\lambda F_p^2$$

when  $m$  is large, this reduces to;

$$C_d = .0037/\lambda F_p^2 \quad \text{with } m \gg 1$$

Thus the lateral misalignment sensitivity is an extremely strong function of primary mirror focal ratio and independent of field angle. Magnification becomes significant when  $0 < m < 2$ .

The image shift  $dY_i$  which is found from;

$$dY_i = (1-m)dY_{cc}$$

is independent of field angle. As with changes in scale introduced by misalignment, its effect on image quality is significant only if the change occurs during an exposure.

Both  $dY_i$  and  $W_c$  are independent of telescope aperture and the tolerances on  $dY_{cc}$  and  $dY_{wo}$  will be the same on an 8-m telescope as on a 10-cm telescope of the same primary mirror focal ratio and secondary magnification if both are diffraction limited.

If coma is kept zero on axis, changes in astigmatism still occur with misalignment. The point of zero astigmatism, previously on axis, splits into two zero astigmatism points whose separation is a function of the magnitude of the misalignment. The total astigmatism at any point in the field is proportional to the product of the distances of that point from both zero astigmatism or nodal points.

Code V optical design program was used to estimate the magnitude of this effect on the Gemini telescope design. First the magnitudes of astigmatism and coma produced by a secondary tilt correcting a decenter were compared. It is expected that the secondary mirror active tip tilt will be required to correct image motion caused by secondary decenters of up to 20 microns. For a secondary decenter of 20 microns a secondary tilt of approximately one arc second is required to

correct the image position. The maximum increase in astigmatism due to this misalignment is less than one percent of the resulting coma at the edge of a six arcminute field.

The effect of using the secondary tip tilt adjustment for tracking was then found. The increase in astigmatism for a four arc second secondary tilt (the maximum expected for tracking), was compared to the resulting coma at a six arcminute field. The results showed that the increase in astigmatism was 16 percent of the resulting coma. Again, this indicates the maximum increase, which is not constant around the edge of the field.

### 3.5 CHOPPING MOTION INDUCED ABERRATIONS.

For IR background cancellation the secondary mirror can be articulated in a square wave tilt pattern between two points on the sky 15 arcseconds apart with an 80% duty cycle at ten Hz. Chopping of the secondary mirror will tilt it about the mirror center of gravity. Because the rotation is about a point other than the neutral point, a residual coma will result. It can be shown that under these conditions coma is the dominant aberration produced. This being the case it is possible to correlate chop angle with both RMS wavefront error and increase in encircled energy at 10 um wavelength. As an example, the on-axis .296 arcsecond diameter for fifty percent encircled energy image, when moved fifteen arcseconds off-axis during chopping, becomes .319 arcsecond diameter at 10 micron wavelength.

For chop angle,  $T_c$  in arcseconds on the sky, the RMS wavefront error,  $W_d$ , in microns may be found from;

$$W_d = T_c 5.43 \times 10^{-3} (\mu\text{m}/\text{arcsec})$$

For chop angle,  $T_c$  in arcsecond on the sky, 50% encircled energy quadrature increase  $dEE$ , in arcseconds may be found from;

$$dEE \approx T_c 7.38 \times 10^{-3} (\text{arcsec}/\text{arcsec})$$

### 3.6 IMAGE SMEAR DUE TO M2 MOTION.

For small tilts and decenters of the secondary mirror, the displacement of the image centroid may be approximated by the linear relationships given below. The coefficients listed are for mirror tilts in arcseconds and decenters in microns.

For mirror tilt,  $T_y$ , image motion  $I_x$  may be found from;

$$I_x = T_y a \quad \text{or} \quad I_x = T_y b$$

For mirror decenter,  $D_x$ , image motion  $I_x$  may be found from;

$$I_x = D_x c \quad \text{or} \quad I_x = D_x d$$

with,

Wavelength	550 nm	2200 nm	10,000 nm	Geometric (chief ray)
<i>a</i> <i>arcsec/arcsec</i>	.256034 (.251268)	.251312 (.251108)	.256084 (.251273)	(.253395)
<i>b</i> $\mu$ <i>m/arcsec</i>	158.885 (155.927)	155.954 (155.828)	155.916 (155.93)	(157.247)
<i>c</i> $\mu$ <i>m/μ m</i>	-7.72169	-7.72474	-7.72654	-7.89
<i>d</i> <i>arcsec/μ m</i>	-0.0124431	-.012448	-0.0124509	-.0127125

For 'a' and 'b' coefficients the first number is for tilt about the mirror vertex, while the second number, in parentheses, is for tilt about the mirror's center of gravity.

### 3.7 ACTIVE CORRECTION USING M2.

Tilt and positioning systems locate the secondary mirror in five degrees of freedom, two in tilt and three in translation. Two axis tilt, and translation in the axial direction each may operate to correct dynamic errors. Translation in the lateral directions operate only in a slow mode. The slow mode will maintain mirror alignment for slowly varying events, such as changing gravity orientation. There will also be a component of tilt error in the initial alignment of the telescope that will be taken out in this mode of operation. The fast modes will be used for chopping, wavefront tilt and telescope structure vibration correction.

The secondary mirror tip tilt will maintain image position whether the error is due to secondary tilt, decenter, or telescope tracking error. If the error is due to a decenter and corrected with a tilt, rotating about a point other than the neutral point, a residual coma will result. It can be shown that under these conditions coma is the dominant aberration produced. This being the case it is possible, for small decenters, to correlate corrected decenter with both RMS wavefront error and increase in encircled energy.

For a small decenter of the secondary mirror,  $D_c$  in microns, the magnitude of secondary mirror tilt,  $T_y$  required to restore the image position from paraxial analysis may be found from;

$$T_y = D_c 5.017 \times 10^{-2} (\text{arcsec}/\mu\text{m})$$

For mirror decenter,  $D_c$  in microns, RMS wavefront error,  $W_d$ , at 2.2  $\mu\text{m}$  wavelength, in microns may be found from;

$$W_d = D_c 3.30 \times 10^{-4} (\mu\text{m}/\mu\text{m})$$

For mirror decenter,  $D_c$  in microns, 50% encircled energy increase dEE, at 2.2  $\mu\text{m}$  wavelength, in arcseconds may be found from;

$$\text{dEE} \approx D_c 1.41 \times 10^{-4} (\text{arcsec}/\mu\text{m})$$

### 3.8 OFF AXIS GUIDING.

When using off-axis guiding a number of potential error sources develop that are not present with on-axis guiding. First, relative motion between on and off-axis images during an exposure causes a smearing of the on-axis image. The relative motion may be due to a number of errors, such as plate scale changes or Cassegrain rotator errors.

### 3.9 PLATE SCALE.

The plate scale, the scale of images in the focal plane, is derived from the effective focal length of the telescope, nominally 128 meters in f/16 configuration. This yields a plate scale of 1.61144 arcseconds per millimeter. The effective focal length of the telescope will change as the radius of curvature of either the primary or secondary mirrors changes.. For both these conditions, the secondary mirror axial position will be used to maintain the focal position, with a residual change in plate scale. Currently, there are no plans to correct for plate scale changes using active optics

For a change in radius of curvature of M1 or M2 the plate scale change in parts per million,  $dPS$ , after focus correction may be calculated from;

$$dPS = S(RMS)$$

with, RMS being the RMS spherical surface error in microns.

S = scale factor, 108.7 ppm/micron for M2 errors, 21.67 ppm/micron for M1 errors

The error budget allowance for plate scale change is 100 ppm. This is divided equally between primary and secondary mirrors with each receiving 70 ppm contribution, added in quadrature.

The plate scale at prime focus with a 14.4 m focal length is 14.32395 arcseconds per mm.

### 3.10 DISTORTION AND ASTIGMATISM.

Distortion is a measure of the difference  $dY$  between the actual image height  $Y$  at which the principle ray strikes the image surface and the image height  $y$  that is predicted by paraxial theory. Third order distortion can be calculated using surface contribution formulas in the same manner as other Seidel aberrations. For the two mirror aplanat:

$$dY/y = a^2(m-B)(m(m^2-2)+(3m^2-2)B)/4m^2(1+B)^2$$

with field angle =  $a$

secondary magnification =  $m = F/F_p$

primary vertex to focus separation/primary focal length =  $B$

This results in a 0.0038% or 38 ppm distortion for the f/16 Gemini telescope design at a 6.0 arcminute field angle.

Astigmatism, as described by the optical path difference between sagittal and tangential rays at the edge of the exit pupil,  $W_{02}$ , is given by;

$$W_{02} = -a^2 D_p ((2m+1)F+n) / 16(m^2 F_p (F_p+n))$$

with field angle =  $a$   
 secondary magnification =  $m = F/F_p$   
 system f/# =  $F$   
 primary f/# =  $F_p$   
 primary diameter =  $D_p$   
 Back focal distance/ primary diameter =  $n$

This results in peak to valley astigmatism in microns of  $-.038a^2$  with field angle in arcminutes. For example, if the optical axis were decentered at the instrument by one arcsecond on the sky, the change in astigmatism at a wavefront sensor six arcminutes off axis would be approximately eight nm P-V.

### 3.11 FIGURE ERRORS, EFFECTS ON IMAGE QUALITY.

Residual mirror figure errors from the figuring and polishing processes will act to reduce the imaging performance of the telescope. A study<sup>7</sup> was made by Breault Research Organization to quantify the effect of mirror figure errors on image quality. To look at their effect, figure errors were divided into low, middle, and high spatial frequencies.

Low spatial frequency errors are those of only a few cycles across the aperture. These errors are typically defined by the low order aberrations of spherical aberration, astigmatism, coma, etc. The distribution of intensity in the focal plane with these errors is highly dependent on the functional form, and well documented in optics literature.

Middle spatial frequencies are defined as those with more than a few cycles across the aperture. These errors, meeting limits of magnitude and correlation length, simply remove power from the point spread function without changing its shape. In general, a figure error with a spatial period  $T$ , directs power away from the central region of the PSF at an angle of  $\lambda/T$ . The following relationship for change in encircled energy  $dEE$ , may be used for middle spatial frequency errors, provided the system is nearly diffraction limited;

$$dEE/EE = (4\pi\sigma/\lambda)^2 \quad \text{for } dEE/EE \leq 0.5$$

with,  $\sigma$  = RMS surface error  
 EE = Encircled energy

Therefore, at infrared wavelengths, where  $(4\pi\sigma/\lambda)^2 \ll 1$ , knowledge of the RMS figure is sufficient to characterize the mirror encircled energy. The contribution of a given surface error to

the change in encircled energy is primarily related to its amplitude and not the value of spatial frequency.

High spatial frequencies, or microroughness, contributes to encircled energy change by the same correlation. However, the distribution of scattered energy is defined by the Bidirectional Reflectance Distribution Function (BRDF). This results in negligible encircled energy changes for scatter characteristics typical of polished glass with a surface roughness of 20 angstroms RMS. Measurement of scattering characteristics is desirable for estimating stray light effects, but scattering is not a significant factor in encircled energy.

### **3.12 REPEATING SURFACE DEFORMATIONS (PRINT-THROUGH), EFFECTS ON IMAGE QUALITY.**

Repeating surface height variations on either M1 or M2 act as a diffraction grating and shift energy to higher orders. This results in multiple satellite images whose separation and intensity are a function of surface error shape, spatial frequency and amplitude as well as wavelength of light.

The effect of print through undulations over the surface of M1 was studied by the Royal Observatory Edinburgh<sup>8</sup>. The analysis done used Fraunhofer diffraction calculations with the pupil modified to incorporate phase variations produced by the undulations. The study concluded that for typical print-through spatial frequencies, the innermost side peaks in the structure of such images occur at radii of many multiples of the diffraction ring radii for the unaberrated system. For hexagonal pattern print-through with amplitudes of 20nm p-v, the strongest individual side peaks have intensities at short wavelengths of 1% of that from the central peak of an unaberrated system.

A specification has been derived based on limiting the background image intensity noise after satellite image subtraction<sup>9</sup>. At spatial frequencies typical of structural or support print-through, surface errors must be below approximately 10 nm rms to meet this specification.

## 4. STRAY LIGHT

### 4.1 EMISSIVITY.

The telescopes will often operate at wavelengths longer than 2.2 microns, where a large source of background radiation is the thermal emission of the telescope and its enclosure. To minimize this radiation at the focal plane requires that detectors see only low emissivity surfaces directly or in reflection. The optimized IR configuration will provide an extremely low emissivity. The Science Requirements Document specifies a requirement of 4% and a goal of 2% emissivity. A study<sup>10</sup> done by Sterling Federal Systems, Inc., used the APART/PADE program to evaluate the effective infrared emissivity of the IR configuration plus enclosure as a function of mirror contamination and at three infrared wavelengths. The conclusions as to the effective emissivity are given here.

It was found that if the coatings are high quality silver, the effective emissivity of the telescope design is below 2%, unless both mirrors are class 500 or dirtier, and that the emissivity decreases slightly with increasing wavelength.

As the mirror contamination increases, half the increase in straylight is due to the increased emissivity of the mirrors. Contamination of the secondary is somewhat more important than the primary. Increasing the secondary mirror contamination has the greatest effect on the amount of enclosure and telescope structure emission that is scattered to the focal plane.

The overall pattern in the focal plane is angularly symmetric, with small oscillations every 45 degrees due to the secondary support struts, with variations up to 0.2%.

When the mirrors are clean, their scatter and telescope emissivity can be moderately reduced by using smoother mirrors. The surface of the secondary is more important than that of the primary in this regard. When mirror contamination is included, however, the dependence of mirror scatter on surface finish is greatly reduced and mirror surface quality has little influence on telescope effective emissivity.

### 4.2 BAFFLES.

The telescope, as a system, can act to concentrate light from both in-field and out-of-field sources. This light acts to nonuniformly raise the background intensity level in the focal plane. Strategically placed stops and baffles are used to limit the amount of unwanted light that reaches the focal plane. A proposed method of baffling the f/16 configuration of the Gemini telescopes is described in this section. Preliminary stray light analysis has been performed<sup>10</sup> by the Dominion Astrophysical Observatory, and the conclusions of that report are also summarized.

The baffle configuration is illustrated in drawing 85-GP-1000-0007. The design is based on the goal that the baffle system can be used for both IR and visible observing modes with only changes in the diameter of the M2 baffle behind the secondary mirror. This requires that the primary baffle not be seen by the IR detector field of view, which was assumed to be 10% larger than the secondary mirror diameter. In addition 30 mm of clearance was provided between the

primary baffle and any 3.5 arcminute field angle ray. For use in the visible the primary baffle must not vignette a 12 arcminute diameter field. Paraxial raytracing yields the following primary baffle dimensions;

Inside diameter of primary baffle (front)	734 mm
Height of primary baffle above primary vertex	4254 mm

The study of the initial configuration shows the degree of attenuation that can be expected at different off-axis angles. Probably the severest stray light conditions occur when observing close to the moon. The preliminary specification limits the stray light to a 0.1% modulation from a 30 degree phase moon 5 degrees off axis. Assuming a dark sky of 23 mag/sq arc sec is brightened to 18.9 mag/sq arc sec by moonlight 5 degrees from the moon at 30 degrees phase, then 0.1% modulation of the sky means no added brightness from scatter amounting to more than 26.4 mag/sq arc sec. If the stray light scatters uniformly over a 12 arcminute field at the detector and the ratio of the detector area to a square arc sec is 14.0 mag, the attenuation needs to be better than 24.4 mag or  $10^{9.8}$ . The analysis done to date show that this level of attenuation will only be possible with careful optimization of the baffle design. Note that this study has made a number of simplifying assumptions as to the size and scatter characteristics of baffle surfaces.

The baffle configuration, using the IR system for visible wavelength observations, is illustrated in drawing 85-GP-1000-0007. The design is based on the goal that the baffle system can be used for both IR and visible observing modes with only changes in the diameter of the M2 baffle behind the secondary mirror. Using the IR system M1 baffle requires that the M2 baffle extend to an outer diameter of 1998 mm to fully shield a 12 arcminute diameter field from direct sky illumination.

### 4.3 VIGNETTING.

Vignetting is described in this section to show the effect of baffles and apertures on the transmittance of the telescope design. The percent transmittance of the telescope is given as a function of field angle in Table 3, both without and with the current M1 baffle.

Field Angle (arcminutes)	Field Diameter (arcminutes)	% transmittance (no baffles)	% transmittance (M1 baffle)	% transmittance (M1 and M2 baffles)
0	0	100	100	100
3	6	99.2	99.2	99.4
6	12	97.5	97.5	97.9
9	18	95.5	86.3	96.1

The IR secondary mirror diameter of 1023 mm obscures 2.25% of the 8 meter M1 aperture. With the M2 baffle fully extended to 1998 mm the obscuration increases to 6.24%.

## 5. ACKNOWLEDGMENTS.

The following people on the Gemini staff contributed to this report; John Roberts, Larry Stepp, Earl Pearson, Joe DeVries, Ron Price. Their analysis and comments are appreciated.

## 6. REFERENCES

- 1) Price R., Gemini report RPT-O-G0032, *Theoretical Active Optics Performance of the Gemini 8M Primary Mirror*
- 2) Huang E., Gemini report TN-O-G0017, *Line of Sight Sensitivity Equations*
- 3) Oschmann J., Gemini specification SPE-S-G0041, *Gemini Error Budget Plan, version 2.1*
- 4) Filippenko A., *The importance of atmospheric differential refraction in spectrophotometry*, PASP, August 1982, Pg 715
- 5) Wetherell W., *General analysis of aplanatic Cassegrain, Gregorian, and Schwarzschild telescopes*, Applied Optics, Vol 11, No 12, 1972
- 6) Wyman C., *Aplanatic Two Mirror Telescopes: A Systematic Study. Cassegrain Configuration*, Applied Optics, Vol 13, No 9, 1974
- 7) Peterson G., Gemini report RPT-BRO-G0016, *The Effect of Mirror Surface Figure Errors on the Point Spread Function of the Gemini Telescope*
- 8) Catalan, Gemini report RPT-O-G0001, *Theoretical Study of the Image Quality of an 8M Primary Mirror Having Print-Through Undulations over the Mirror Surface*
- 9) Hickson, P., *Proposed Image Quality Specification for the Gemini Telescopes*, June 3, 1992
- 10) Dinger A., Gemini report RPT-SFS-G0020, *Thermal Emissivity Analysis of a GEMINI 8-meter Telescopes Design*
- 11) Morbey C., Gemini report RPT-DAO-G0040, *Preliminary Stray Light Analysis for Gemini*

## APPENDIX A

The following is a Code V listing of the telescope optical prescription. Surfaces one through four are the secondary support structure vanes. Surface five is an obstruction to obstruct the sky from the image surface. Surface six is an aperture at the edge of the primary mirror. It prevents rays that would fall off of the primary from being traced. Surface seven is the primary mirror. Surface eight is the secondary mirror. Note that it is the aperture stop for the system. Surface nine represents the primary mirror and is reentered to include the central hole. Surface ten is a dummy surface.

```

          RDY      THI  RMD   GLA      CCY  THC  GLC
> OBJ:   INFINITY  INFINITY  AIR          100 100
1:   10.00000    0.000000          100 100
  CON:
  K : -40.538000  KC : 100
  XDE: 0.000000  YDE: -208.466000  ZDE: 0.000000  DAR
  XDC: 100      YDC: 100      ZDC: 100
  ADE: 0.000000  BDE: 0.000000  CDE: 0.000000
  ADC: 100      BDC: 100      CDC: 100

2:   10.00000   2290.594000          100 100
  CON:
  K : -40.538000  KC : 100
  XDE: 0.000000  YDE: 208.466000  ZDE: 0.000000  DAR
  XDC: 100      YDC: 100      ZDC: 100
  ADE: 0.000000  BDE: 0.000000  CDE: 0.000000
  ADC: 100      BDC: 100      CDC: 100

3:  -10.00000    0.000000          100 100
  CON:
  K : -40.538000  KC : 100
  XDE: 0.000000  YDE: -208.466000  ZDE: 0.000000  DAR
  XDC: 100      YDC: 100      ZDC: 100
  ADE: 0.000000  BDE: 0.000000  CDE: 0.000000
  ADC: 100      BDC: 100      CDC: 100

4:  -10.00000   14.029000          100 100
  CON:
  K : -40.538000  KC : 100
  XDE: 0.000000  YDE: 208.466000  ZDE: 0.000000  DAR
  XDC: 100      YDC: 100      ZDC: 100
  ADE: 0.000000  BDE: 0.000000  CDE: 0.000000
  ADC: 100      BDC: 100      CDC: 100

5:   INFINITY  13000.000000          100 100
6:   INFINITY   277.772750  AIR          100 100
7:  -28800.00000 -12539.326000  REFL AIR          100 100
  ASP:
  K : -1.003756  KC : 100
  IC: YES      CUF: 0.000000  CCF: 100
  A :0.000000E+00  B :0.000000E+00  C :0.000000E+00  D :0.000000E+00
  AC: 100      BC: 100      CC: 100      DC: 100

```

STO: -4193.06850 12539.326000 REFL AIR 100 100  
 ASP:  
 K : -1.612898 KC : 100  
 IC : YES CUF: 0.000000 CCF: 100  
 A :0.000000E+00 B :0.000000E+00 C :0.000000E+00 D :0.000000E+00  
 AC : 100 BC : 100 CC : 100 DC : 100

9: -28800.00000 4000.000000 AIR 100 100  
 ASP:  
 K : -1.003756 KC : 100  
 IC : YES CUF: 0.000000 CCF: 100  
 A :0.000000E+00 B :0.000000E+00 C :0.000000E+00 D :0.000000E+00  
 AC : 100 BC : 100 CC : 100 DC : 100

10: -1915.43000 0.000000 AIR 100 100  
 IMG: -1915.43000 0.000000 AIR 100 100

#### SPECIFICATION DATA

EPD 7899.56628  
 DIM MM  
 WL 2200.00  
 REF 1  
 WTW 1  
 CWL 2200.00  
 XAN 0.00000  
 YAN 0.00000  
 VUX 0.00000  
 VLX 0.00000  
 VUY 0.00000  
 VLY 0.00000

#### APERTURE DATA/EDGE DEFINITIONS

CA  
 REX S1 OBS L'ULL' 1754.191000  
 REY S1 OBS L'ULL' 5.000000  
 ADX S1 OBS L'ULL' -1515.802002  
 ADY S1 OBS L'ULL' -1451.639038  
 ARO S1 OBS L'ULL' 43.761002  
 REX S1 OBS L'ULR' 1754.191000  
 REY S1 OBS L'ULR' 5.000000  
 ADX S1 OBS L'ULR' 1515.802002  
 ADY S1 OBS L'ULR' -1451.639038  
 ARO S1 OBS L'ULR' -43.761002  
 REX S2 OBS L'UUL' 1754.191000  
 REY S2 OBS L'UUL' 5.000000  
 ADX S2 OBS L'UUL' -1515.802002  
 ADY S2 OBS L'UUL' 1451.639038  
 ARO S2 OBS L'UUL' -43.761002  
 REX S2 OBS L'UUR' 1754.191000  
 REY S2 OBS L'UUR' 5.000000  
 ADX S2 OBS L'UUR' 1515.802002  
 ADY S2 OBS L'UUR' 1451.639038  
 ARO S2 OBS L'UUR' 43.761002  
 REX S3 OBS L'LLL' 1754.191000

REY S3 OBS L'LLL' 5.000000  
ADX S3 OBS L'LLL' -1515.802002  
ADY S3 OBS L'LLL' -1451.639038  
ARO S3 OBS L'LLL' 43.761002  
REX S3 OBS L'LLR' 1754.191000  
REY S3 OBS L'LLR' 5.000000  
ADX S3 OBS L'LLR' 1515.802002  
ADY S3 OBS L'LLR' -1451.639038  
ARO S3 OBS L'LLR' -43.761002  
REX S4 OBS L'LUL' 1754.191000  
REY S4 OBS L'LUL' 5.000000  
ADX S4 OBS L'LUL' -1515.802002  
ADY S4 OBS L'LUL' 1451.639038  
ARO S4 OBS L'LUL' -43.761002  
REX S4 OBS L'LUR' 1754.191000  
REY S4 OBS L'LUR' 5.000000  
ADX S4 OBS L'LUR' 1515.802002  
ADY S4 OBS L'LUR' 1451.639038  
ARO S4 OBS L'LUR' 43.761002  
CIR S5 LIN' 4006.476400  
CIR S5 OBS L'BAF' 600.000000  
CIR S6 4000.000000  
CIR S6 OBS 600.000000  
CIR S8 511.969400  
CIR S8 OBS 77.550000

## INFINITE CONJUGATES

EFL 0.1280E+06  
BFL -0.0119  
FFL -0.8780E+06  
FNO 16.2034  
IMG DIS 0.0000  
OAL 19582.3957  
PARAXIAL IMAGE  
HT 0.0000  
ANG 0.0000  
ENTRANCE PUPIL  
DIA 7899.5663  
THI 0.1126E+06  
EXIT PUPIL  
DIA 1020.7304  
THI -16539.3260

## APPENDIX B

This appendix is excerpted from the M1 polishing contract as of 5/19/94.

### 2. General Requirements.

2.1. Introduction. This specification details the requirements for the generating, polishing and figuring of the Blanks.

2.2. Configuration. Contractor shall generate, remove the central core, and polish the Blanks, converting them into finished Mirrors, which shall conform in all respects to the requirements specified in Drawing No. 85-GP-2000-0003. Such drawing is attached to, and is hereby made a part of, this Exhibit C.

### 3. Polished Surface Specifications.

3.1. Definition. The polished surface of the Mirrors is defined as "Surface A" on Drawing No. 85-GP-2000-0003.

3.2. Test Regions. Surface A, as defined in Section 3.1, above, is divided into three zones as defined below:

Zone 1: The annular section on Surface A having an outer diameter of at least 8080 mm and an inner diameter of 8000 mm.

Zone 2: The annular section on Surface A having an outer diameter of 8000 mm and an inner diameter of 1220 mm.

Zone 3: The annular section on Surface A having an outer diameter of 1220 mm and an inner diameter of no greater than 1190 mm.

#### 3.3. Surface Figure of Revolution.

3.3.1. Equation for the Polished Surface A. Surface A shall be a conic surface of revolution described by the following equation:

$$Z = Y^2 / (R(1 + (1 - (1 + K)Y^2/R^2)^{0.5}))$$

where:

Z = sagitta of the optical surface  
 R = Paraxial Radius of Curvature  
 K = conic constant  
 Y = distance from the optical axis

3.3.2. Conic Constant. The value of the conic constant, K, used in the above equation shall be:  
 $K = -1.00376 \pm 0.0005$ .

3.3.3. Paraxial Radius of Curvature. The Paraxial Radius of Curvature of Surface A shall be:  
 $R = 28,800 \pm 30$  mm.

3.3.4. Vertex Location and Tilt of Optical Axis. The axis of revolution of Surface A shall be coincident with the geometrical axis of the Mirror, Datum Axis A on Drawing No. 85-GP-2000-0003 to within the following tolerances:

(a) Axis Tilt - The axis of revolution of Surface A shall be parallel to the geometrical axis of the Mirror, Datum Axis A, to within 5 arc minutes; and

(b) Vertex Decenter - The vertex of Surface A shall be located on the geometrical axis of the Mirror, Datum Axis A, within a cylindrical tolerance zone of 2 mm diameter.

### 3.4. Surface Quality.

3.4.1. Surface Roughness. Surface A shall be pitch polished to a 20 A rms or better surface roughness.

3.4.2. Surface Imperfections. Contractor shall use its best efforts to minimize the number of imperfections in Surface A. Within Zone 2 of Surface A no surface imperfections of surface area larger than 1.0 square millimeter shall be allowed, and a maximum of two (2) defects of surface area 1.0 square millimeter or less, including scratches less than or equal to 5 mm in length, are allowed within any 70 mm by 70 mm square area of Surface A. Bubbles present in the Blanks upon their delivery to Contractor are not included in this requirement. Within Zone 2, no more than 5 scratches of length greater than 5 mm are allowed within any 3000 mm by 3000 mm square area of Surface A.

3.5. Theoretical Telescope Optical System. The optical performance of the Mirrors is to be calculated by Contractor as though the Mirror were incorporated into a theoretical optical system as described below and illustrated in Figure 1 (Theoretical Telescope Optical System), attached to and made a part of this Exhibit C. All point spread function and encircled energy calculations required by this Exhibit C shall be based on the Theoretical Telescope Optical System.

3.5.1. Aperture Stop. For purposes of optical performance calculations, the aperture stop of the system shall be 8,000 mm outside diameter and 1220 mm inside diameter, and shall be located 280 mm above the vertex of the Mirror.

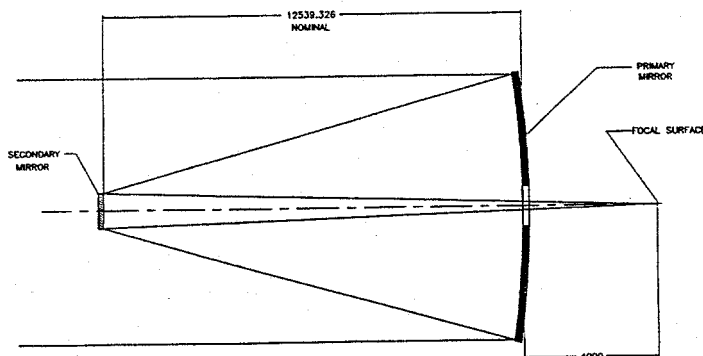


FIGURE 1. THEORETICAL TELESCOPE OPTICAL SYSTEM

3.5.2. Secondary Mirror. (a) The surface of the theoretical secondary mirror is defined by the following radius of curvature and conic constant:

Radius of Curvature = -4193.0685 mm;

Conic Constant = -1.612898.

(b) The nominal distance between the vertices of the Mirror and secondary mirror shall be 12,539.326 mm; except that such distance can be adjusted slightly by Contractor during computer analysis to maintain the required focal surface position.

3.5.3. Focal Surface Position. The focal surface of the Theoretical Telescope Optical System shall be located 4,000 mm behind the primary Mirror vertex, as illustrated in Figure 1.

### 3.6. Surface Figure Accuracy - Required Level.

3.6.1. Accuracy for Zone 2. (a) Contractor shall use its best efforts to make Surface A as smooth as possible, free of ripple, zones and local bumps.

(b) The figure of Surface A within Zone 2 shall be such that the encircled energy concentration of the calculated point spread function of the Theoretical Telescope Optical System, including diffraction effects at a wavelength of 2200 nm, meets the following requirements:

Encircled Energy	Maximum Angular Diameter
50%	0.067 arc second
85%	0.207 arc second

(c) The figure of polished Surface A within Zone 2 shall be such that the encircled energy concentration of the calculated point spread function of the Theoretical Telescope Optical System, including diffraction effects at a wavelength of 550 nm, meets the following requirements:

Encircled Energy	Maximum Angular Diameter
80%	0.10 arc second

(d) The calculation of encircled energy shall take into account the effects of all surface figure errors that significantly affect (as determined by AURA) the encircled energy distribution. Therefore, the optical test information which describes the Mirror figure that is used in the encircled energy calculation shall include all spatial frequencies that will significantly affect (as determined by AURA) the calculated results, as discussed further in section 5.1.2, below.

(e) Measurement uncertainty in the calculation of encircled energy shall be considered, and shall be included in the calculation of encircled energy, as described in Section 5.2, below.

3.6.2. Accuracy for Zones 1 and 3. The surface figure of the polished surface A shall extend smoothly into Zone 1 and Zone 3 with no abrupt changes or discontinuities.

3.6.3. Intensity of Satellite Images. If regular patterns of repeating surface features exist in polished Surface A, such features will act as a diffraction grating to preferentially diffract energy from the point spread function into satellite images outside the central core of the point spread function. The maximum intensity of any such satellite image between 0.25 and 2 arc seconds radial distance from the center of the point spread function, at any wavelength between 500 nm and 3000 nm, shall not exceed:

$$I_s \leq I_c r^3 (5 \times 10^{-4})$$

where  $I_s$  is the intensity of the satellite image,  $I_c$  is the central intensity in the point spread function, and  $r$  is the radial distance of the satellite image from the center of the point spread function in arc seconds.

### 3.7. Surface Figure Accuracy - Goal Level.<sup>1</sup>

3.7.1. Accuracy for Zone 2. (a) To meet the goal level of accuracy, the figure of Surface A within Zone 2 shall be such that the encircled energy concentration of the calculated point spread function of the

<sup>1</sup>See Section 2.1.1 of the Statement of Work (Schedule B).

Theoretical Telescope Optical System, including diffraction effects at a wavelength of 550 nm, meets the following requirements:

Encircled Energy	Maximum Angular Diameter
85%	0.08 arc second

(b) The calculation of encircled energy shall take into account the effects of all surface figure errors that significantly affect (as determined by AURA) the encircled energy distribution. Therefore, the optical test information which describes the Mirror figure that is used in the encircled energy calculation shall include all spatial frequencies that will significantly affect (as determined by AURA) the calculated results, as discussed further in section 5.1.2, below.

(c) Measurement uncertainty in the calculation of encircled energy shall be considered, and shall be included in the calculation of encircled energy, as described in Section 5.2, below.

#### 4. Mirror Support.

4.1. Polishing. Contractor shall support the Mirrors during polishing in a manner that prevents the formation of high spatial frequency surface features or defects.

4.2. Testing. (a) The Mirror shall be supported during Pre-final Inspection testing in a manner identical to the support that will be provided by the Mirror Cell during telescope operation, as provided in Section 8.2.2 of the Contract.

(b) If the Metrology Mount does not provide support identical to that of the Mirror Cell, as provided in paragraph 4.2(a), above, any errors produced by such deviation shall be treated as described in Section 5.2, below. Any such deviations shall be approved by AURA. If Contractor can demonstrate that the errors produced by the deviation can be calculated with sufficient accuracy, AURA may permit subtraction of the errors from the interferometry data, and only the uncertainty in the calculations shall be treated as a measurement error.

4.3. Active Force Adjustment. (a) The support mechanisms of the Metrology Mount may have active force control to remove low order (as determined by AURA) aberration terms in Surface A. AURA will provide Contractor with a list of nominal mechanism support forces. During testing, Contractor may change each mechanism support force specified by AURA by up to  $\pm 100$  newtons from the nominal forces. Contractor shall determine the optimum force set to correct errors in Surface A. Once the optimum force set is determined, all tests evaluating the figure of Surface A, the Paraxial Radius of Curvature, and the Conic Constant shall be performed by Contractor with such optimum force set. Support mechanism forces shall not vary from the optimum force set by more than  $\pm 1$  newton during Pre-final Inspection testing.

(b) If the force sensors incorporated into the Metrology Mount do not have sufficient resolution in adjusting the Mirror figure, AURA may permit Contractor to analytically adjust the measured surface figure of the Mirror by adding a calculated theoretical correction to the measured Mirror figure as supported on the Metrology Mount; provided, however, that the theoretical correcting force at any support location must be within the range of  $\pm 3$  newtons.

#### 5. Optical Testing.

##### 5.1. Required Tests.

5.1.1. Full Aperture Interferometry. (a) Contractor shall test the entire Surface A (all zones of Surface A) of the Mirror by interferometry at a wavelength of 632.8 nm using a Null Corrector. The Null Corrector shall be used during such test in the manner specified in the Acceptance Test Plan, and to the extent not inconsistent with the provisions of this Contract, as specified in the Proposal. The projected size of the detector pixels on Surface A of the Mirror shall be no larger than 35 mm. Contractor shall calculate the point spread function from the surface figure information derived during the interferometric test.

(b) No spatial "smoothing" of the surface map of Surface A (including all zones of Surface A) shall be allowed, other than that provided by averaging of multiple measurements. At least 99.7% of the data points contained within all zones of Surface A shall be included in the calculations. Any data points to be excluded from the map of Surface A, plus data dropouts, shall not exceed 0.3%.

5.1.2. Sub-aperture Interferometry. (a) Contractor shall verify the surface smoothness of the polished Surface A by sub-aperture interferometry, which shall be capable of measuring all surface errors that significantly (as determined by AURA) affect the encircled energy calculation, but were not adequately measured by the full aperture interferometry. The aperture size and resolution of the sub-aperture interferometry shall allow measurement of surface errors having spatial frequencies ranging from the upper limit of frequencies measured by the full aperture interferometry, up to the highest spatial frequency having an amplitude large enough to significantly (as determined by AURA) affect the encircled energy calculation; provided, however, that the projected size of the detector pixels on Surface A of the Mirror shall be no larger than 4 mm.

(b) The size and number of test areas for the sub-aperture interferometry will be chosen by AURA to provide coverage of all radial zones of Surface A, and to provide 100% coverage of Zone 3 of Surface A. Test area locations for each radial zone of Surface A will be specified by AURA at the time of the Pre-final Inspection test by AURA.

5.1.3. Second Test Method. An additional and completely independent test method, not requiring a null corrector, shall be used by Contractor to verify the Paraxial Radius of Curvature and Conic Constant of Surface A. Such test shall provide for Paraxial Radius of Curvature measurements to an accuracy of  $\pm 10$  mm, and Conic Constant measurements to an accuracy of  $\pm 0.0005$ .

5.1.4. Satellite Image Test. Contractor shall develop a test method that is capable of verifying compliance with the requirements of Section 2.6.3. of this Exhibit C.

5.2. Testing Accuracy. (a) For each test required to verify compliance with this specification, expected errors that might occur because of test equipment inaccuracies, test parameter uncertainty, air refraction and vibration effects during testing, calculation approximations, or other error sources, shall be predicted by Contractor. The predicted errors shall be evaluated by Contractor in terms of relative probability of occurrence, and shall be set at a level such that there shall be a 90% probability that the actual errors will be less than the predicted errors. These predicted errors shall be added to the measured or calculated test values, as appropriate, and the combination of the measured or calculated test values, plus the predicted errors, shall meet the requirements of this Exhibit C.

(b) In evaluating the expected errors, Contractor may remove any errors that can be shown by appropriate calculations to be correctable by the active optics system, provided that the total correction for all removed errors can be accomplished without extending the range of active force magnitude at any one actuator by more than 50 newtons. A summary of the error evaluation for each testing procedure shall be included in the Acceptance Test Plan.

## APPENDIX C

This appendix contains the proposed secondary mirror polishing specification.

### 2. General Requirements.

2.1. Introduction. This specification details the requirements for the generating, polishing and figuring of the Blanks.

2.2. Configuration. Contractor shall polish the Blanks, converting them into finished Mirrors, which shall conform in all respects to the requirements specified in Drawing No. 85-GP-3200-0004. Such drawing is attached to, and is hereby made a part of, this Exhibit C.

### 3. Polished Surface Specifications.

3.1. Definition. The polished surface of the Mirrors is defined as "Surface A" on Drawing No. 85-GP-3200-0004.

3.2. Test Regions. Surface A, as defined in Section 3.1, above, has an outer diameter of 1022 mm and an inner diameter of 169 mm.

#### 3.3. Surface Figure of Revolution.

3.3.1. Equation for the Polished Surface A. Surface A shall be a conic surface of revolution described by the following equation:

$$Z = Y^2/2R + (1+K)Y^4/8R^3 + 3(1+K)2Y^6/48R^5$$

where:

Z = sagitta of the optical surface  
 R = Paraxial Radius of Curvature  
 K = conic constant  
 Y = distance from the optical axis

3.3.2. Conic Constant. The value of the conic constant, K, used in the above equation shall be:  
 $K = -1.612898 \pm 0.001$ .

3.3.3. Paraxial Radius of Curvature. The Paraxial Radius of Curvature of Surface A shall be:  
 $R = -4193.0685 \pm 5$  mm.

3.3.4. Vertex Location and Tilt of Optical Axis. The axis of revolution of Surface A shall be coincident with the geometrical axis of the Mirror, Datum Axis A on Drawing No. 85-GP-3200-0004 to within the following tolerances:

(a) Axis Tilt - The axis of revolution of Surface A shall be parallel to the geometrical axis of the Mirror, Datum Axis A, to within 5 arc minutes; and

(b) Vertex Decenter - The vertex of Surface A shall be located on the geometrical axis of the Mirror, Datum Axis A, within a cylindrical tolerance zone of 1.0 mm diameter.

#### 3.4. Surface Quality.

3.4.1. Surface Roughness. Surface A shall be pitch polished to a 20 A rms or better surface roughness.

3.4.2. Surface Imperfections. Contractor shall use its best efforts to minimize the number of imperfections in Surface A. Within Surface A no surface imperfections of surface area larger than 1.0 square millimeter shall be allowed, and a maximum of two (2) defects of surface area 1.0 square millimeter or less, including scratches less than or equal to 5 mm in length, are allowed within any 70 mm by 70 mm square area of Surface A.

3.4.3. Subsurface Damage. Contractor shall use its best efforts to minimize subsurface damage in Surface A. Within Surface A no increase in surface roughness due to subsurface damage shall be evident after 2.0 micron depth of surface removal using ion figuring techniques after delivery of the Mirror.

3.5. Theoretical Telescope Optical System. The optical performance of the Mirrors is to be calculated by Contractor as though the Mirror were incorporated into a theoretical optical system as described below and illustrated in Figure 1 (Theoretical Telescope Optical System), attached to and made a part of this Exhibit C. All point spread function and encircled energy calculations required by this Exhibit C shall be based on the Theoretical Telescope Optical System.

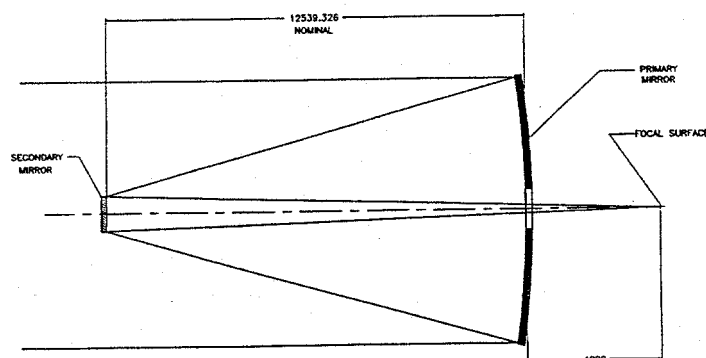


FIGURE 1. THEORETICAL TELESCOPE OPTICAL SYSTEM

3.5.1. Aperture Stop. For purposes of optical performance calculations, the aperture stop of the system shall be the 1022 mm outer diameter of the Secondary Mirror.

3.5.2. Primary Mirror. (a) The surface of the theoretical primary mirror is defined by the following radius of curvature and conic constant:

$$\text{Radius of Curvature} = 28,800 \text{ mm};$$

$$\text{Conic Constant} = -1.00376.$$

(b) The nominal distance between the vertices of the Mirror and primary mirror shall be 12,539.326 mm; except that such distance can be adjusted slightly by Contractor during computer analysis to maintain the required focal surface position.

3.5.3. Focal Surface Position. The focal surface of the Theoretical Telescope Optical System shall be located 4,000 mm behind the primary Mirror vertex, as illustrated in Figure 5.

3.6. Surface Figure Accuracy - Required Level.

3.6.1. Accuracy (a) Contractor shall use its best efforts to make Surface A as smooth as possible, free of ripple, zones and local bumps.

(b) The figure of Surface A shall be such that the encircled energy concentration of the calculated point spread function of the Theoretical Telescope Optical System, on axis, including diffraction effects at a wavelength of 2200 nm, meets the following requirements:

Encircled Energy	Maximum Angular Diameter
50%	0.067 arc second
85%	0.207 arc second

(c) The figure of Surface A shall be such that the encircled energy concentration of the calculated point spread function of the Theoretical Telescope Optical System, on axis, including diffraction effects at a wavelength of 550 nm, meets the following requirements:

Encircled Energy	Maximum Angular Diameter
80%	0.10 arc second

(d) As a goal, the figure of Surface A shall be such that the encircled energy concentration of the calculated point spread function of the Theoretical Telescope Optical System, including diffraction effects at a wavelength of 550 nm, meets the following requirements:

Encircled Energy	Maximum Angular Diameter
85%	0.08 arc second

(e) The calculation of encircled energy may be done after removal of errors in the form of the first ten (10) standard Zernike terms only. The maximum error subtraction shall be equivalent to 100 nm RMS mirror surface error. A maximum error subtraction at any single point shall be equivalent to 0.65 microns mirror surface error.

(f) The calculation of encircled energy shall take into account the effects of all surface figure errors that significantly affect (as determined by AURA) the encircled energy distribution. Therefore, the optical test information which describes the Mirror figure that is used in the encircled energy calculation shall include all spatial frequencies that will significantly affect (as determined by AURA) the calculated results, as discussed further in section 5.1.2, below.

(g) Measurement uncertainty in the calculation of encircled energy shall be considered, and shall be included in the calculation of encircled energy, as described in Section 5.2, below.

3.6.3. Intensity of Satellite Images. If regular patterns of repeating surface features exist in polished Surface A, such features will act as a diffraction grating to preferentially diffract energy from the point spread function into satellite images outside the central core of the point spread function. The maximum intensity of any such satellite image between 0.25 and 2 arc seconds radial distance from the center of the point spread function, at any wavelength between 500 nm and 3000 nm, shall not exceed:

$$I_s \leq I_c r^3 (5 \times 10^{-4})$$

where  $I_s$  is the intensity of the satellite image,  $I_c$  is the central intensity in the point spread function, and  $r$  is the radial distance of the satellite image from the center of the point spread function in arc seconds.

#### 4. Mirror Support.

4.1. Polishing. Contractor shall support the Mirrors during polishing in a manner that prevents the formation of high spatial frequency surface features or defects.

4.2. Testing. (a) The Mirror shall be supported during final Inspection testing in a manner identical to the support that will be provided by the Tip-Tilt system during zenith pointing telescope operation, as provided in the Contract.

(b) If the Metrology Mount does not provide support identical to that of the Tip Tilt system, as provided in paragraph 4.2(a), above, any errors produced by such deviation shall be treated as described in Section 5.2, below. Any such deviations shall be approved by AURA. If Contractor can demonstrate that the errors produced by the deviation can be calculated with sufficient accuracy, AURA may permit subtraction of the errors from the interferometry data, and only the uncertainty in the calculations shall be treated as a measurement error.

## 5. Optical Testing.

### 5.1. Required Tests.

5.1.2. Sub-aperture Interferometry. (a) Contractor shall verify the surface smoothness of the polished Surface A by full or sub-aperture interferometry, which shall be capable of measuring all surface errors that significantly (as determined by AURA) affect the encircled energy calculation. The aperture size and resolution of the sub-aperture interferometry shall allow measurement of surface errors having spatial frequencies ranging up to the highest spatial frequency having an amplitude large enough to significantly (as determined by AURA) affect the encircled energy calculation; provided, however, that the projected size of the detector pixels on Surface A of the Mirror shall be no larger than 0.5 mm.

(b) In the absence of full aperture testing, the size and number of test areas for the sub-aperture interferometry will be chosen to provide coverage of all areas of Surface A. Sub-aperture interferograms shall be combined into an equivalent full aperture interferogram. Contractor shall calculate the point spread function from the surface figure information derived during this interferometric test.

5.1.3. Second Test Method. An additional and completely independent test method shall be used by Contractor to verify the Paraxial Radius of Curvature and Conic Constant of Surface A. Such test shall provide for Paraxial Radius of Curvature measurements to an accuracy of  $\pm 1$  mm, and Conic Constant measurements to an accuracy of  $\pm .0005$ .

5.1.4. Satellite Image Test. Contractor shall develop a test method that is capable of verifying compliance with the requirements of Section 2.6.3. of this Exhibit C.

5.2. Testing Accuracy. For each test required to verify compliance with this specification, expected errors that might occur because of test equipment inaccuracies, test parameter uncertainty, air refraction and vibration effects during testing, calculation approximations, or other error sources, shall be predicted by Contractor. The predicted errors shall be evaluated by Contractor in terms of relative probability of occurrence, and shall be set at a level such that there shall be a 90% probability that the actual errors will be less than the predicted errors. These predicted errors shall be added to the measured or calculated test values, as appropriate, and the combination of the measured or calculated test values, plus the predicted errors, shall meet the requirements of this Exhibit C.